Land cover change detection analysis for the Atok area with special emphasis on chrome mining development

Ramoshweu Melvin Sethobya (Student No: 1920591)

Supervisor: Dr Solomon Newete

Co-Supervisor: Dr Elhadi Adam

This report is submitted to the Faculty of Science, University of the Witwatersrand, in Partial fulfillment of the requirements for the degree of Masters by Coursework and Research Report in Environmental Sciences

University of the Witwatersrand, Johannesburg, South Africa
School of Animal, Plant and Environmental Sciences

November 2020

Acknowledgments:

First, I would like to thank the Lord for the gift of life. I dedicate this work to my grandparents: Kagalagala Mack le Mme Elisa Ramaesele Sethobja. I would also like to acknowledge my family, in particular my Mom and my siblings, my wife and my son for all the support. To my supervisor, Dr Solomon Newete for his untiring and steadfast support throughout this work, as well as providing guidance, useful insights and for assisting when I needed him most, I`m deeply grateful. I would also like to acknowledge the following people: Dr Elhadi Adam, Dr Emmanuel Sakala and Dr Janine Cole for their insights, advice and words of encouragements. I acknowledge the Council for Geoscience for financial support, provision of software and for affording me the time to conduct the study. Lastly, I would also like to thank all the colleagues at the Council for Geoscience, with whom we shared ideas, knowledge, struggles, prayers, and words of encouragement.

*TO **GOD** BE ALL THE GLORY!!*

Declaration:

I declare that this thesis is my own unaided work**.** It is being submitted for the degree of Masters (by Coursework and Research Report) in Environmental Sciences at the University of the Witwatersrand, Johannesburg. This work has never been submitted for any other degree or professional qualification before.

Ramoshweu Melvin Sethobya

12 November 2020

Acronym	**Description**
AVHRR	Advanced Very High Resolution Radiometer
CVA	Change Vector Analysis
ESA	European Space Agency
ETM+	Enhanced Thematic Mapper
DN	Digital Numbers
LCC	Land Cover Change
LG6	Lower Group 6 Chromite seam
LULC	Land Use Land Cover
MLC	Maximum Likelihood Classification
MSS	Multispectral Scanner System
NDVI	Normalized Difference Vegetation Index
NLC	National Land Cover
NIR	Near infrared
PGM	Platinum Group Minerals
RF	Random Forest
SVM	Support Vector Machine
SPOT	Satellite Pour l'Observation de la Terre
UG2	Upper Group 2

ABSTRACT

The main focus of this research study was to quantify temporal land cover changes (LCC) around the Atok area in Sekhukhune District, Limpopo Province, over a period of four years. The influence of chrome mining expansion on land cover changes was mapped using Sentinel-2 imageries acquired in 2016 and 2019 using the Maximum Likelihood Classifier (MLC) and Support Vector Machine (SVM) classification algorithms. Normalized difference vegetation index (NDVI) was used to establish correlation between the change analysis results with classification results.

The overall accuracies of the 2016 and 2019 Sentinel-2 image classifications using the MLC were 83% (with kappa value of 0,77) and 80% (with kappa value of 0,75) respectively, while those of the SVM classifier were 84% (with a 0,78 kappa coefficient) and 81% (with a 0,76 kappa coefficient) respectively, showing that the SVM outperformed the MLC by a 1% margin.

The chrome mining operations grew by 1,6% from an average of 2,3% in 2016 to 3,9% in 2019, which is an increase of 314.5 hectares over the period of four years. Vegetation cover decreased by an average of 3,3% (648,6 ha) during this period. A moderate increase of 3,8% was recorded for dry areas, owing to exposures due to stripping and open cast mining in the new chrome mining operations. Further analysis of land cover types revealed the inter-relations of the change scenarios between the chrome mining class and other land cover types available in the study area. NDVI results highlighted areas of increased dry soil exposures and areas with major losses in vegetation cover, which are attributable to development of new chrome mining operations. Mapping of land cover change using Sentinel-2 imageries has proven robust in effectively highlighting the impact of chrome mining activities and its expansion on the local landscape quality and environmental degradation within the area.

Table of contents

Table of Figures

1. CHAPTER ONE: INTRODUCTION AND STUDY BACKGROUND

1.1 Introduction

Mining serves as a source of raw materials and minerals required for industrial and domestic use in many countries throughout the world. In South Africa, the mining industry remains the most important economic sector and plays a key role in attracting foreign investment by creating a platform for leading global enterprises (Sorensen, 2011). In 2018, mining contributed R356bn or 7.3% to the country`s GDP, which accounted for 25% of the country’s total export earnings (InvestSA, 2020). Chrome ore is amongst the most essential metal ores currently mined in the country. Over the past decade, chrome mining development experienced a gradual growth in Southern Africa. The growth in chrome ore exports from South Africa is mainly driven by a yearly consumption growth rate of approximately 3,7% worldwide, the bulk of which is led by China (Engineering News, 2019). South Africa possess about 70% of the total chrome reserves found around the world (Sharaky, 2014). Most of this comes from the Bushveld Igneous Complex, which produces about 75% of the world's ferrochrome (Africa Mining IQ, 2019). In 2017, the country produced over half of the world`s total production of chrome ore (Africa Mining IQ, 2019).

Most mining activities are infamous for their inherent pollution footprints on the surrounding environment. Surface chrome mining operations are no different and leaves a legacy of huge levels of adverse environmental pollution behind. Growth in the chrome mining operations typically leads to a severe alteration of the landscape dynamics, which includes a substantial decrease in landscape quality (Coetzee *et al.*, 2020), water quality (Mavunda, 2016), decrease in vegetation growth and an increase in the overall environmental pollution.

Remote sensing applications have widely been used to analyze and uncover the causes, trends, development and extent of the land cover changes, to facilitate the decision-making process for the effective implementation of mitigation measures of adverse environmental impacts (Xiuwan, 2002; Mundia and Aniya, 2005). These applications have also been used for monitoring, maintenance, natural resources management and local spatial planning, with an overall objective of ensuring environmental sustainability. This study investigates the use of thematic satellite images (Sentinel-2) for visualization of impacts of continual expansion of surface chrome mining operations on land cover change over an area, during a four years period. The study presents measurements of LCC through a descriptive assessment of changes in different land cover classes as impacted by a gradual growth and expansion of surface chrome mining operations. Sentinel-2 imagery was used as a platform to evaluate the Land cover change (LCC) around the Atok area and its surroundings. The Maximum Likelihood Classifier (MLC) and Support Vector Machine (SVM) algorithms were used to highlight the LCC in the area from the year 2016 to 2019. The Normalized Difference Vegetation Index (NDVI) change over the assessment period was used as supplementary information to complement the classification results. Change analysis was conducted to quantify the land cover change caused by growth and expansion of chrome mining operations within the study area.

1.2 Background

Surface mining usually leads to environmental degradation due to the various landscape disturbances such as air pollution, increase in soil erosion, visual disturbance, loss of arable land, degradation of vegetation productivity and contamination of water resources (Ololade *et al.*, 2008, Mensah *et al.*, 2015 and Coetzee *et al.*, 2020). The effects of surface mining activities create conditions that exacerbates an increased imbalance in the ecological well-being of a landscape, which in turn could result in severe impacts on the wellbeing of local plants, animals, organisms and human communities.

Quantification of spatial and temporal land cover change in an area offers opportunities to understand the extent and intensity of localized environmental degradation caused by those changes. Proper quantification of land change scenario within the landscape will improve our understanding of the -temporal changes as they relate to developmental growth and adequately inform policy direction and spatial planning (Verburg *et al.*, 2009). Local LCC data is important as feeder information for understanding the current worldwide changes, which would be used to inform future decision-making on ecological management and environmental monitoring (Hassan *et al*., 2016). Therefore, the monitoring of the short-term landscape change dynamics in a severely altered area may provide the basis for prediction of projected long-term ecological, social and natural resources degradation, as well as provision of possible solutions for mitigation of the environmental impacts of the changes in an area.

A severe deterioration in the quality of available land resources can lead to several unwanted implications that may lead to scarcity of land resources, such as improper use, illegal or unregulated use of land resources, institution of civil land claims, improper land apportionments, civil unrest, etc.

1.3 Research questions

This study is based on the hypothesis that continual expansion of the existing chrome mining operations severely affects land cover change dynamics within the study area. Therefore, this study seeks to answer the questions listed below, to test the hypothesis.

- What is the effects of chrome mining activities on LCC in the Atok area between the years 2016 and 2019?
- Is medium resolution Sentinel-2 imagery adequate for LCC mapping?

1.4 Research aims and objectives

The main aim of the study was to quantify temporal land cover changes (LCC) of the Atok area using Remote Sensing tools.

Objectives

The specific objectives of this study were to:

- Identify chrome mining activities through use of Maximum Likelihood Classification and Support Vector Machine supervised classification techniques.
- Compare the capabilities of Maximum Likelihood Classification and Support Vector Machine supervised classification techniques for land cover change mapping.
- Quantify LCC that occurred due to the growth and expansion in the chrome mining activities during the assessment period.

1.5 Significance of the study

Successful completion of this study would add to currently available of knowledge on the use of MLC and SVM classification algorithms for LCC mapping. Although the study uses the common remote sensing analysis applied in sequential LCC mapping, it offers relatively new information pertaining to impacts of chrome mining development on land cover change dynamics in South Africa, for which there is only little information in literature. Availability of LCC maps is critical for spatial planning, natural resources monitoring, landscape management and conservation, as well as for the running of monitoring programs at all governance administrative levels.

This study intends to fill gaps pertaining to research work conducted for quantifying impacts of surface chrome mining activities on LCC dynamics in the mining areas of Southern Africa. It also contributes to the understanding of driving factors of LCC locally and serves as feeder information for implementation of LULC change models at a regional scale. It is expected that findings of this study would serve as a great value addition into establishment of standardized methodologies for mapping chrome mining impacts on LCC, which would be used for determination of adequate environmental mitigation solutions, and to assist in future spatial planning for rural and semi-urban settlements. Moreover, the LCC datasets could be used as basis for understanding factors that contribute to reduction in the quality of land resources as well as essential information for development of plans for rehabilitation of mining impacted landscapes.

2. CHAPTER TWO: STUDY LOCALITY

This chapter provides an introduction to the study locality, detail the area geology, local landscape dynamics, the mining history, and offer an understanding of chrome mining development within the study area and its impacts on the landscape.

2.1 Study area and the local mining history

The study area is situated between Latitudes -24,200° to -24,300° and Longitudes 29,790° to 30,010°. The area falls within the Fetakgomo Local Municipality, within the Sekhukhune District in Limpopo province (Figure 1). The study area covers an area totalling 19,653 hectares and it is a site that has been subjected to intensive mining of Platinum Group Minerals (PGM) and chrome ore for the past three decades. The area has a rich mining history. One of the most notable reference points within the study area is the Atok platinum mine. The mine is renowned for being one of the oldest platinum mines in the country, having started operations around the 1960s and one of the first mines to explore the UG2 and Merensky PGM-bearing reefs (Fogg and Cornellisson, 1993). The mine operates the Brakfontein Merensky, the Middlepunt Hill UG2 shafts plus an opencast section at Klipfontein. In 2017, Bokoni mine stopped its mining operations due to financial liquidity problems, but plans are now afoot to resume the platinum mining operations. Chrome mines have also operated in the area before. The Jadglust mine was a small opencast mine that was exploiting near surface chromite seams. It ran operations in the early 1970s and continued for a period of 3-8 years (Lee and Perry, 1988). The Jadglust operation was economically productive and during its heydays, and was rated amongst the best producing chrome mines in South Africa (Fogg and Cornellisson, 1993). The chromite seams being exploited extends over 200km in distance from Dwars River in the far-east near Steelpoort, to Bogalatladi village in the west. Most of the chrome mining activities highlighted in this study emanates from an extension of the reef previously exploited by the Jadglust chrome mine. Some of the newer, more formalized and well-structured operations are found near Tsibeng village and up in the mountains south of the village. The study area encompasses a number of rural villages, several rugged mountains and a regional arterial road connecting the towns of Polokwane in the west and Burgersfort in the east. The perennial Olifants River (locally known as the Lepelle River) cuts across the study area, treading eastwards. Two other smaller and seasonal tributaries exist within the study area, namely the Mphogodiba and Rapholo Rivers, feeding into the larger Olifants River.

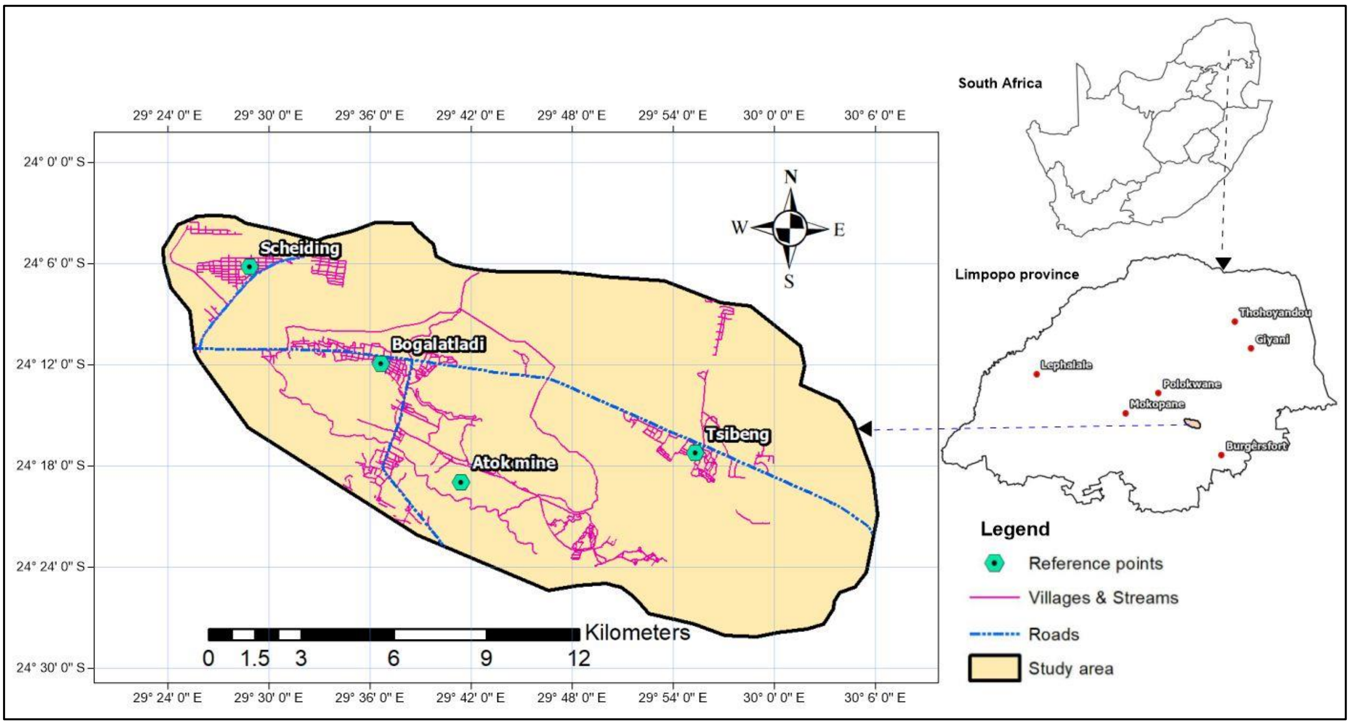

Figure 1. A study location map showing the area around the Atok mine in Sekhukhune District, Limpopo Province.

2.2 Climate and terrain

The area being investigated enjoys a pleasant climate throughout the year. The summer period can be relatively hot, with temperatures occasionally reaching highs between 32-36° Celsius. It enjoys a mean annual temperature of 23° Celsius and an average annual rainfall of 600ml (Mpandeli *et al.*, 2015). Most of the rainfall mainly occurs in summer and winter is usually the driest season, with most of the available shrub lands, woodland and vegetation losing their canopies. Topographically, the area boats a succession of rugged mountainous features, as well as other relatively well vegetated slopes and small valleys, although most of the existing residential infrastructure lies on gentle slopes or relatively flat plains. The area is relatively well vegetated with green leafy trees covering most of the mountains on the western and the far south-eastern side. The mid-section of the area is covered by rugged and dry mountains, which generally exhibits sparse distributions of vegetation at the top.

2.3 Area geology

Our focus area is located mainly within the eastern limb of the Bushveld Igneous complex, which is a large layered intrusion covering a surface area approximately 65,000km^2 (Eales and Cawthorn, 1996). The Bushveld complex is made up of several limbs, which are: the western, northern, southern, and the eastern limbs, and each limb is made up of a number of domains (areas) which are referred to as zones.

Geologically, the study area is covered mainly by successions of mafic rocks such as norites, anorthosites and pyroxenites, some of which comprises within their layered successions the various Platinum Group Minerals (PGM) which includes economically mineable commodities such as Chromium, Platinum, Palladium, Rhodium, Iridium, etc. The chromite seams being exploited within the selected study area are part of the Upper group 2 (UG2) and the Lower Group 6 (LG6) chromite seams. The UG2 seam is known to extend approximately 230km laterally (East-West) within the eastern limb of the Bushveld (McLaren and De Villiers, 1982).

The major economic chromite deposits found within the Bushveld Igneous Complex occurs as two types: stratiform or the podiform types. Stratiform type chromite deposits occur as parallel zones or elongated seams (Sciarone, 1998). Their layering is consistent and they also exhibit considerable lateral continuity. This explains the strong lateral continuity and surface representation of the chrome ore mining operations, which are spread continually over a linear stretch of area, extending along strike from the eastern edge almost all the way through the western edge of the study area.

2.4 Chrome mining

Due to the rapid industrialization in the world, natural resources are being over-exploited to satisfy the growth in demand for metal commodities in countries such as China, India, and other developing countries in the world (Africa Mining IQ, 2019). Chromite is one of the metal ores in high demand in the ferro-alloy industries. It is a highly valuable metal mainly used in different industrial applications for production of anticorrosive super alloys, stainless steel and as an additive in the production of industrial chemicals such as paints.

Early mining of chromite was conducted in small pits and trenches, where only conventional hand tools were utilized. However, as demand grew, large scale open pit workings were developed, as well as mechanical underground mining, which required use of heavy mining equipment (Africa Mining IQ, 2019). The ore being mined is found at different grades, which are consumed differently due to varying levels of demand. The high demand from stainless and other alloy steel industries has necessitated for an uptake in chrome ore at various grades, including low grade ores (Africa Mining IQ, 2019). According to KPMG (2018), stainless steel demand is the major driver for demand of ferrochrome and chrome ore commodities. The worldwide stainless steel production market is currently led by China (KPMG, 2018), see Figure 2. Therefore, the high demand from the stainless steel industry hugely influences the price of chrome ore exported from South Africa, which in-turn induces growth and expansion of chrome mining operations locally, to ensure adequate supply. As such, the continual expansion in chrome mining operations within our study locality over the past few years comes as no surprise. Within the study area, most resources situated close to the surface are mined via open-pit mining to an approximate depth 50m. Several small and medium sized mining companies have opened chrome exploiting operations within the study, including some small scale operators and illegal artisanal miners. Figure 3 shows some of the operations captured from within the area, some of which are conducted within villages and up in the mountains, while some operations are run by small scale and illegal miners.

2.5 A summary of the chapter

This chapter offered an introduction to our site locality, to build an understating of the site conditions, including the local area setting, the land cover types available around the area and the climatic conditions. The geological setting within which the site exists allows for an understanding for the existence of numerous chrome mining operations. The chapter also brings to the fore the rich mining history due to abundance of PGM deposits in the area, which forms the basis for the continual growth and expansions of chrome mining operations within the study area. The choice of the study area is solely based on the premise that mining activities often imparts severe environmental impacts and landscape degradation. The landscape degradation is related to land cover change mapping, which is described in detail in the next chapter.

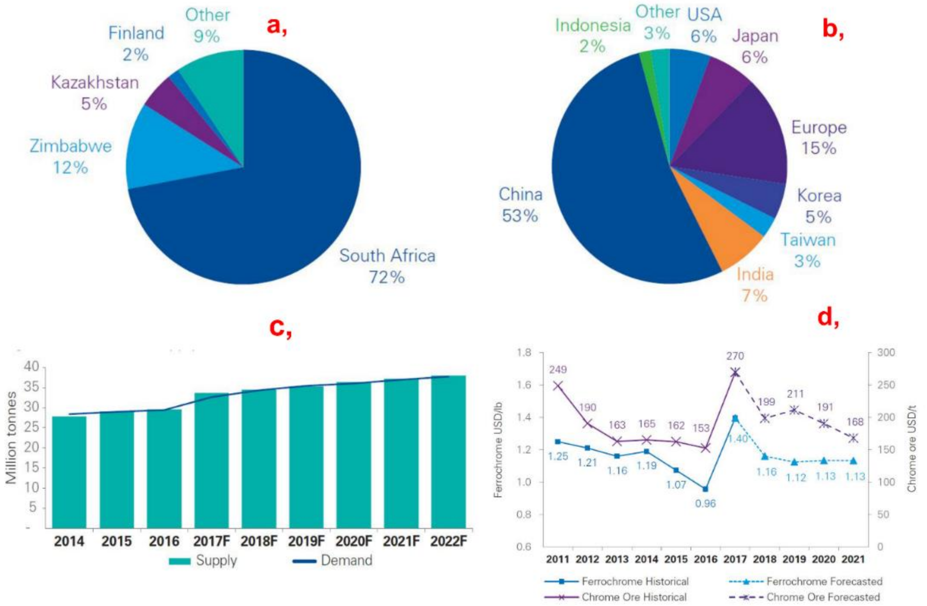

Figure 2. Chrome mining information. a, Chromite reserves in the world, b, Stainless steel production by country, c, Chrome ore supply and demand, and d, Historical and forecasted chrome ore and ferrochrome prices. Graphics courtesy of KPMG report (2018).

Figure 3. Site images depicting chrome mining operations around the Atok mine area, a, The yellow outline shows a chrome ore stockpile at one of the mines, b, new operations in the mountains, c, an excavator working in a shallow chrome mining operation. d, some of the chrome mining operations are found in close proximity to residential units (local`s homes). Images collected during site visits.

3. CHAPTER THREE: LITERATURE REVIEW

This chapter provides a brief history of land cover change mapping and an introduction to the principles, methodologies and technologies commonly applied for LCC studies. It also describes various research works that applied the technique used herein, and highlights various shortcomings and the trade-offs that must be accounted for in any research that involves these methodologies.

3.1 Background of land cover mapping

Land cover mapping is a commonly used and significant application of remote sensing because of its ability to provide valuable scientific results, guidance for policy change and decision making in environmental monitoring (Verburg *et al.*, 2009; Melesse and Abtew, 2016). The use of remotely sensed images for the extraction of LULC targets has an extensive history, which extends before introduction and commission of the Landsat satellites (Sohl *et al.*, 2010). Land cover, by definition, refers to the physical material that covers the surface of the earth, which are often categorized as different classes such as vegetation, open-water, built-up or residential, wetlands, forests, etc. In terms of their description and purpose, land cover and land use are different. Land use explains the purpose for which a patch of land is utilized or serves, such as agriculture, recreation, conservation, mining, etc. Land use and Land cover are very closely related, and are usually analyzed together for purposes of obtaining a broader perspective on material changes of an area. Those types of studies are known collectively as LULC studies. Different land cover types usually exhibits different phenology. Some of the major land cover classes found within our study area includes residential areas, vegetation types, shrubs, patches of cultivated crops and woodlands, bare, fallow and dry lands, and mining operations. A more detailed South African national land cover map of 2018 (DEA, 2019) was used as a basis for initial assessment of the land cover scenario in the area and for development of the class schemes.

Periodic land cover change analysis is usually applied for monitoring of the impacts of land cover changes, which affects the spatial extent and magnitude of ground based features (Sakai *et al.*, 2015). Land cover data are frequently used to offer information relating to periodical landscape transformations, assessment and monitoring of landscape condition. The work covered in the present study is based on pioneering works in the field of land cover mapping conducted by writers such as Giri (2016), Thompson (1996), Zhu et al. (2008) and many others. These works covered very significant topics such as early development of land cover models, standardization procedures, selection procedures and criterion, sensitivity thresholds for class separations and fundamental principles in development of land cover classes for national and regional land cover mapping.

Availability of easily accessible, good quality, accurate and latest countrywide land cover products forms the basis of a thriving LCC research sector. There is usually a lack in availability of datasets used for sustainable and effective land use and land cover monitoring, more especially in underdeveloped and a number of developing countries throughout the world, mainly due to lack of resources, unstable economies and conflicts. In South Africa, several national land cover products have been developed, since 1994. These includes the National Land Cover 94 (NLC 94), NLC 2000, NLC 2005 and NLC 2013. Each subsequent product was an improvement of the previous version, with reviews of the sampling methodologies, technologies utilized and involved the use of higher or better resolution imagery. Ngcofe and Thompson (2015) reported on the status of land cover mapping in South Africa over the period between the years 1994-2015. Their report detailed the processes and methods applied in classification of land cover types, datasets and classification schemes used in the development of the National Land Cover products over the time span. To date, the latest available land cover product is the NLC 2018, released by the Department of Environmental Affairs (DEA, 2019). These products are useful in many ways: as basis for comparison, improvements of land cover classifications, developments of class schemes, change detection mapping and time series analysis and for LCC mapping studies by various sectors of the economy such as forestry and earth sciences, agriculture and environmental monitoring agencies.

3.2 Impacts of mining on a landscape

Large scale and rapid land cover changes coupled with over-exploitation of natural resources have the potential to cause severe negative environmental impacts (Suhari and Siebenhüner, 1993). A huge body of scientific research studies has been conducted on the social impacts of mining in South Africa, although much of these is related to impacts due to mining of commodities such as Coal, Platinum and Gold mining. However, there is very little literature on the impacts of chrome mining developments on land cover change in South Africa.

Landscape degradation is one of the major forms of environmental impact caused by surface extraction of ore or open pit mining, and is a subject of high concern for many communities. The work covered in this study involves surface chrome mining operations, which usually have a major impact on land degradation. Surface mining methods can lead to several landscape disturbances such as erosion, air pollution, topographic change, removal of vegetation, and impacts on water resources. When left unattended and unabated, such disturbances may lead to major environmental risks. The World Bank`s report sustainable development in 1994, noted that mining has the ability to contribute immensely to high levels of landscape deterioration, degradation and pollution in areas with abundant natural resources, if compliance to environmental policies is neglected and legislation is poorly enforced (World Bank, 1994). A total disregard for landscape degradation can lead to an increase in natural and man-made risks.

Land cover conversion/transformation is a topic widely researched using time series analysis and spatio-temporal mapping for purposes of land use monitoring. Several researchers have produced land cover transformation mapping at regional or national scales. Wessels et al. (2004) studied the impacts of human-induced land degradation using a time series approach. Their study quantified the influence of changes in rainfall patterns and NDVI changes, and its contribution to man-made landscape degradation and analysed the interrelationships between vegetation decline, vegetation productivity and levels of degradation in areas as influenced by change in rainfall patterns. This highlights the value of land cover transformation research, which is particularly more important for the agricultural industry. Other forms of land cover transformations may result in degradation (Mbiwa, 2018) and/ regeneration of forest landscapes (Southworth, 2004) or habitat disturbances and species movements (Gillespie *et al.,* 2008; Nagendra *et al.,* 2013).

Numerous efforts have been made to map land degradation in specific areas within South Africa, using a variety of satellite datasets such as with Landsat TM datasets (Turyahikayo, 2015; Münch *et al.,* 2017) and AVHRR (Wessels *et al.,* 2004) and High resolution SPOT imagery

(Tanser and Palmer, 1999). Several studies have also been conducted in South Africa to measure the impacts of extractions of commodities such as platinum mining (Ololade *et al.*, 2008), iron ore, limestone, coal and marble on land cover in an area. Results from such studies have been used by government in various ways i.e., influence environmental monitoring policy, in shaping regulatory framework and use as input data for development of land cover map products. Other studies have highlighted the topic of erosion of social identity for people living in close proximity to mining operations, which also involves exposures to high risk of serious health impacts due to exposure to harmful levels of environment pollution.

3.3 Use of Sentinel-2 imagery for land cover mapping

Medium resolution Sentinel-2 imagery has been used for LULC studies, land cover analysis and other environmental monitoring applications, since its launch in 2015. Several studies have been conducted to demonstrate the successes recorded with use of Sentinel-2 imagery for land cover change analysis, vegetation monitoring, aquatic studies, glacial studies and various other applications (Sothe *et al.,* 2017; Makaya *et al.,* 2019 and Phiri *et al.,* 2020).

Thanh Noi and Kappas (2018) successfully demonstrated capabilities of Sentinel-2 imagery for land cover mapping, obtaining a good overall accuracy in the range 90% - 95%. Their study compared and analyzed performances of various classifiers such as the Random Forest, the K-Nearest Neighbors algorithm and Support Vector Machine for land use and cover classifications. Although their study focused primarily on comparing various classification algorithms, an expression of Sentinel-2 data capabilities for land cover mapping was also established. The study by Clerici et al. (2017) further demonstrates the adequacy of both medium resolution Sentinel-1 and Sentinel-2 imagery. Their study explored the integration of radar data (Sentinel-1) and multispectral (Sentinel-2) datasets, for land cover change classification and produced good overall accuracies for the combined Sentinel-1 and 2 imageries. An overall accuracy of 88.75% with a kappa coefficient of 0.86 was attained, with all the land cover classes considered obtaining producer accuracies higher than 80%. These types of studies justify the application of medium resolution Sentinel-2 images for land cover monitoring studies.

3.4 Techniques and technology typically applied in LCC studies

The methods, technologies and quality of datasets used for analysis of LCC is continuously improving. This study draws on the use of remote sensing techniques and their application in environmental monitoring. Continuous development of remote sensing techniques through use of satellite imagery and similar products has influenced growth in land cover mapping research and its related applications (Mbiwa, 2018).

A number of classification algorithms are applied to map and quantify various facets of landscape change. Supervised and unsupervised classification algorithms are predominantly applied for highlighting changes on the earth's surface. Other machine learning algorithms such as deep learning, cluster analysis, artificial neural networks, anomaly detection, principal components analysis, etc., are also applied in various fields to study change in very complex landscapes.

In this study, supervised classification methods, through application of SVM and MLC algorithms are used to map land cover change over the study period from 2016-2019. Fichera et al. (2012) conducted a study similar to the current one. Their study characterized land cover change dynamics for an area in Southern Italy during a fifty-year period (1954–2004) using SVM and MLC algorithms. Their study found that LCC patterns were primarily linked to natural such as earthquakes, floods or tsunamis and social processes such as urbanization and rapid population growth.

Several research studies have been conducted using this approach with varying levels of success (Taati *et al.,* 2015; Szuster *et al.,* 2011). Most of the studies were carried out to assess the performances of different classification algorithms, sometimes pitted against each other to measure their levels of accuracies. Adam et al. (2014), used Rapid-Eye imagery to assess the performance of the RF and SVM classifiers in LULC classification of a coastal environment, to determine the efficacy in application of different RapidEye bands on classification outputs. Results from their study found that the RF and SVM classifiers performed comparatively similarly. The study achieved overall accuracies of 93.07% and a 0.92 kappa coefficient for the RF, while the SVM classifier obtained a 91.80% overall accuracy with a kappa coefficient of 0.92. Similarly, Lu and Weng (2007) conducted a research study using image classification methods and techniques applied to improve classification performances. Their study outlined reviews of the performances of various classification techniques and results of comparisons of various algorithms when compared. Their research focused on grouping different classification approaches such as per-pixel, subpixel, per-field, contextual-based, knowledge-based, and a combination of multiple classifiers to study accuracy levels obtained with application of each approach. Using this method, their research showed that combinations of different classification algorithms is effective for improvement of overall classification accuracies.

Similar studies have been conducted by other researchers who focused on specific combinations/comparison of different classification algorithms such as Random forest and MLC, or SVM and MLC (Deilmai *et al.,* 2014; Rimal *et al.,* 2020), as is the case in the current study. Thanh Noi and Kappas (2018) compared random forest (RF) algorithm, k-nearest neighbor, and support vector machine classifiers for use in land cover classification on Sentinel-2 imagery. Their results showed that the SVM classifier produced the highest overall accuracy (95,45% on average), with the least sensitivity to training sample size, followed closely by the RF (94,5% on average) and k-nearest neighbors (kNN) classifiers (94,10% on average). Results from such studies further reinforces the notion that the SVM classifier is usually a superior classifier, when pitted against most other similar classifiers, for land cover mapping studies.

Utilization of multiple classifiers for classification of land cover change offers plenty of advantages such as improved classification accuracies, the ability of certain classifiers to better classify certain land cover classes than others and the addition of more ancillary information for adaptive class weight selections.

3.5 Summary of the chapter

This chapter offered an analytical summary of relevant literature to the current study, as well as summarizing important themes covered in historical land cover mapping studies. Impacts of mining on landscape degradation were outlined, with specific examples related to the current study offered. In the following sections, the typical methodologies and technological equipments typically applied for LCC studies were explored, which gave a basis for the use of remote sensing applications selected in this study. Once these are outlined, a sound basis is created for the quantification of land cover change that occurred within our study area during the assessment period. The next chapter will outline the methods and materials required for data acquisition, processing, and the descriptions of parameters and theoretical principles behind the applications of the selected classification techniques. The methods to be used in data analysis are also outlined and explained to give an understanding of how the results will be derived.

4. CHAPTER FOUR: METHODS AND MATERIALS

This chapter presents the basis, methods used and theoretical principles that underpins applications of the methodology used in the study. First, the introduction to remote sensing and its application for LCC mapping is presented. Then, the subsequent topics deals with acquisition of the dataset, pre-processing and the methods used for its analysis. This background provides a gateway into analysis of the classification results and creates conditions for attainment of the research objectives.

4.1 Remote sensing and GIS

According to Tomlinson et al. (2011), remote sensing refers to the science of obtaining information about an object or area without being in physical contact with it. This is made possible by use of various types of sensors, which are deployed to acquire information about the area. Remote sensing technology with its multi-temporal and multi-spectral observations allows for both short-term and long-term monitoring to assess, quantify and predict spatial change or growth (Taubenböck and Esch, 2011). For the current study, medium -resolution Sentinel-2 imagery was used to map temporal changes in land cover within the study area. The study is conducted following the process detailed in Figure 4.

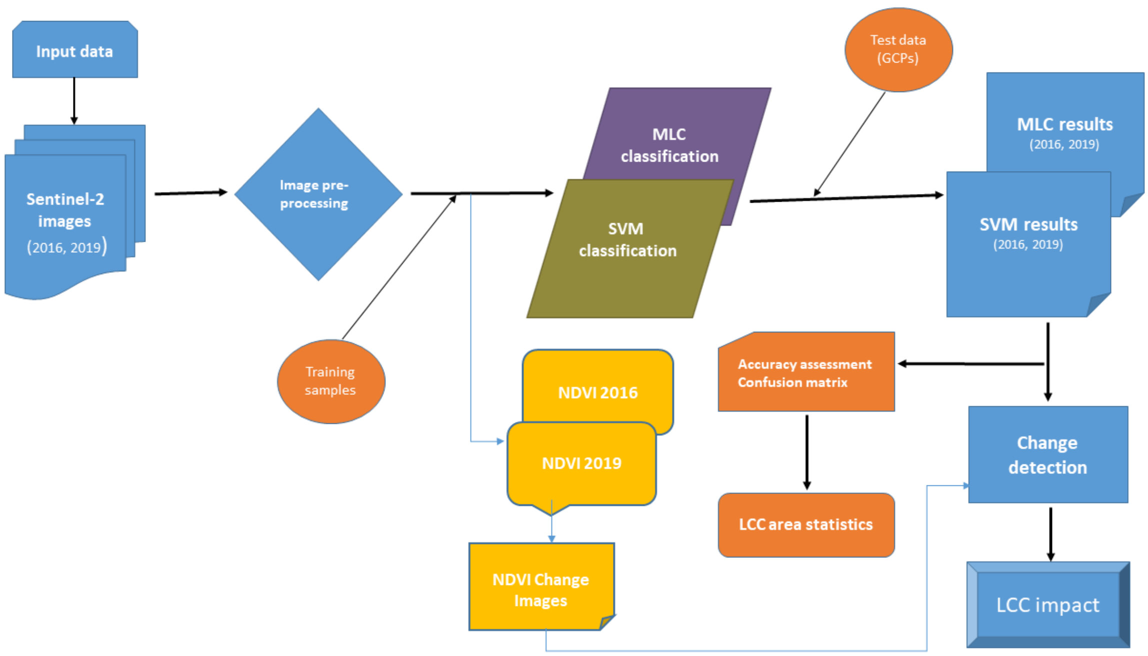

Figure 4. Flowchart diagram showing the steps followed to conduct this study.

4.2 Resolution

4.2.1 Spatial, spectral and temporal resolution

There are different types of resolutions which are essential in remote sensing. Spatial resolution in imagery refers to the number of pixels used in construction of a digital image (Huang *et al.*, 2013). Sentinel-2 images are useful for LCC classification as they exhibit a reasonable spatial accuracy, which is capable of meeting important requirements such as discrimination of subtle features at an appreciable levels of clarity. Spectral resolution of a sensor refers to the ability to resolve finer features within different wavelengths of the electromagnetic spectrum. (Dlamini *et al.*, 2019). It can be expressed as the width of the recorded spectral bands. There are a number of spectral bands in use, which includes the red, green, blue bands, and NIR, Mid-IR, thermal, bands, etc. Only certain bands or a combination of bands better reflects some features on the ground. The greater the number of the bands, the more detailed the information extracted, which enables the analyst to effectively discriminate between different and smaller objects. Temporal resolution describes the ability of a sensor to collect imagery of the same area of the earth's surface at different periods of time (Emetere, 2019). By studying temporal changes, an analyst can compare spectral characteristics of features and analyze the changes over a measured period of time.

4.2.2 Radiance and reflectance

Radiance

Radiance is a radiometric measure that defines the amount of light that is emitted or reflected by a medium. According to Ackerman (2011), reflected solar irradiance represents the radiance of importance in optical remote sensing. This distinction amplifies the importance of the reflectance characteristics of each land cover feature, which can be identified by calculating its radiance character. The spectral reflectance of a surface object is can be defined as follows:

$$\rho(\lambda) = E_r(\lambda) / E_i(\lambda)$$

Where, $E_r(\lambda)$ represents the reflected spectral energy from the surface object and $E_i(\lambda)$ represents the spectral irradiance incident of the surface object. Spectral reflectance curves are used to indicate the amount of energy reflected by certain surface features at a specific wavelength.

The spectral reflectance curves functions as indicators for the presence of certain features on the earth`s surface as they are related to their spectral attributes.

Radiometric calibration

Radiometric calibration is an image pre-processing step used to improve quality of resultant images for scientific analysis (Chander *et al.,* 2009). A radiometric calibration is required for conversion of digital numbers data from image pixels into surface reflectance units. Equations and parameters for the conversion of calibrated Digital Numbers (DN) to at-sensor radiance or Top-Of-Atmosphere (TOA) reflectance are sensor specific to type the sensor used, as in Sentinel-2 satellite sensor for the current study.

4.3 Sentinel-2 satellites data

European Space Agency (ESA) `s Sentinel-2 satellite was launched in 23 June 2015, and contains two satellites for land monitoring with a full systematic coverage of land surface at worldwide level. The Sentinel-2 Multi-Spectral Instrument (MSI) satellites provides good resolution imagery useful for monitoring of changes in land surface conditions, at a high revisit time (5 days at the Equator) and covers a wide swath width of 290 km (Clerici *et al.,* 2017). Sentinel-2 consists of 13 spectral bands (VNIR, NIR and SWIR region bands) making it more valuable for mapping and discriminating between different species of vegetation (Forkuor *et al.,* 2018). Sentinel-2 has a good combination of both spatial and spectral resolution, adequate for land cover classification. The spatial resolution of Sentinel-2 satellite is categorized as moderate resolution (10m for VNIR bands and 60m for the SWIR bands), which is better than that of freely available Landsat 7 Enhanced Thematic Mapper (ETM+) imagery which has 30m spatial resolution for bands 1 to 7 and 15m for band 8 (panchromatic). Availability of the newer multispectral sensors such as Sentinel-2 has resolved the data accessibility limitation created by high resolution hyperspectral sensors which are exorbitantly expensive and difficult to access for research purposes (Sibanda *et al.,* 2017). This study preferred use of Sentinel-2 imagery over other freely available datasets such as Landsat Thematic Mapper imagery, because Sentinel-2 has a higher spectral and spatial resolutions, which are more suited for land cover assessment purposes. Although a number of studies reported equal or similar performances between Sentinel-2 and Landsat 8 imagery products for land cover mapping studies when using the main visible and near-infrared bands, this study chose Sentinel-2 imagery on the basis of better pixel resolution. The study by Forkuor et al. (2018) did report on a slightly better performance of all Sentinel-2 bands compared to Landsat 8 in classification using a number of machine learning algorithms. When compared to Landsat TM imagery, the Sentinel-2 imagery is only better as it has additional red-edge bands at wavelengths 704,1, 740,5 and 782,8 nm, which are useful for monitoring of green leafs and chlorophyll content in vegetation. For this study, only the visible and near infrared bands were used, without any one of the red-edge bands as the focus was solely placed on identification and discrimination of different land cover classes. For identification of vegetation changes, an index was considered, which utilized only the red band (B4) and the enhanced infrared band (B8A). With particular reference to our site, the object of interest i.e., the size of the chrome mine workings generally ranges between 5-30m thick, rendering Sentinel-2 imagery better compared to Landsat imagery for identification of such features due to its superior spatial resolution.

4.4 Data acquisition

Sentinel-2 images were used in this study to evaluate the impacts of chrome mining on the LCC and one of its advantages is that it has a reasonably short temporal resolution of 5 days, which is more suitable for continuous monitoring of vegetation health (Mashamba, 2017). Sentinel-2 medium resolution imagery were downloaded from the ESA`s Sentinel-2's Scientific Data Hub. Single date imagery was downloaded, each one (1) for the years 2016 and 2019. Winter (dry) season images were preferred, because cloud cover is usually very less during the winter season. Table 1 outlines information of the satellite imagery used in compilation of the study.

4.5 Pre-processing

Each image was subjected to a pre-processing procedure before any classification was conducted. During pre-processing, the images were corrected, individually, using the Sen2Cor plugin installed in ESA`s SNAP software. Sen2Cor is a pre-processing plugin designed specifically to correct and adjust Sentinel-2 Level 2A imagery datasets. It performs the atmospheric, terrain and cirrus correction of Top-Of-Atmosphere Level 1C input data (Chatziantoniou, *et al.*, 2017). Upon processing, Sen2Cor creates Bottom-Of-Atmosphere (Level 2A), terrain and atmospherically corrected surface reflectance images.

The images were geo-coded using Shuttle Radar Topography Mission (SRTM) 30m DTM data to correct for topographic effects and projected onto the WGS84/UTM 35S system for the study area. Sentinel-2 bands in the visible and near infrared (NIR) range of the electromagnetic spectrum were preferred for this analysis (VNIR region bands). The bands have 10m and 20m resolutions respectively, see Table 1. Sentinel-2`s SWIR and TIR bands have larger pixel sizes, with a lower spatial resolution of 60m. These bands are usually resampled to 10m using one of the visible range band images, to ensure good spatial resolution of the merged multispectral datasets. Individual band images were merged into multilayer composites for each year (RGB 432). Each pre-processed image was cropped to the margins of the study area for ease of reference and to ensure that processing efficiency is improved.

4.6 Band selections

Sentinel-2 has many bands in the VNIR and its main application is for vegetation mapping. MSI Sentinel-2 imagery has unique spectral bands and a higher signal to noise ratio which is particularly useful for environmental monitoring studies (Drusch *et al.*, 2012). Image band selections used for the current studies are described in the paragraphs below.

4.6.1 RGB

In this study, Sentinel-2's natural colour image i.e., Red: band 4 (665 nm), Green: band 3 (560 nm) and Blue: band 2 (460 nm) were used for the classification. The bands were then merged to form RGB composites used for selection of training data and to perform the classifications.

4.6.2 NDVI

The normalized difference vegetation index (NDVI) is a standard index used in remote sensing applications to assess the presence and condition of green vegetation in satellite imagery. "NDVI is measured using values derived from visible and near-infrared light reflected by vegetation. Healthy vegetation absorbs most of the visible light that fall on it and reflects a large portion of near-infrared light" (Earth Lab 2019, p. 1). NDVI was computed using the Red band 4 (665 nm) and the enhanced infrared band 8A (865 nm). For this study, NDVI is chosen for its ability to describe the basic characteristics of a healthy or unhealthy vegetated patch of area. In this study NDVI was used as supplementary data, to highlight vegetation loss/bare soil changes in the locations where new chrome mining operations are established and for highlighting the change scenario during the assessment period. The value ranges for NDVI are from

-1 to a maximum of 1. High NDVI values represents denser and greener vegetation while low NDVI values (below zero) represents less green or other coloured vegetation/dry leafs/rocky areas. A substantial change in the low NDVI values during the assessment period would indicate the potential influence of human-induced changes, such as expansions of chrome mining operations which leads to heavy metal induced stress that reduces the leaf chlorophyll levels or general vegetation health. NDVI is also applied to reduce impacts of topographic effects and illumination when doing change detection analysis (Herrmann *et al.*, 2005). For areas with expansions/growth in chrome mining operations, NDVI is expected to be very low, due to clearing of vegetation and heavy metal enrichment (Fe, Cr, Mn, Al, etc.) and an increase in exposed soils/rocks. The NDVI is calculated as follows:

$$\mathrm{NDVI} = \frac{(\mathrm{NIR} - \mathrm{RED})}{(\mathrm{NIR} + \mathrm{RED})}$$

Where, *RED* = Red reflectance value (Band 4) and *NIR* = near infrared reflectance value (Band 8).

Table 1. Characteristics of the Sentinel-2 satellite imagery and bands used for this study. Table modified from ESA (2016).

Sensor ID	Path/Row	Acquisition date	Cloud (%)	Band information		
				Bands	**Wave-length (nm)**	**Spatial resolution**
Sentinel-2A	169/77	2016/07/16	3%	Blue (B2)	490	10
				Green (B3)	560	10
				Red (B4)	665	10
				NIR (B8A)	865	20
Sentinel-2A	169/77	2019/07/01	1%	Blue (B2)	490	10
				Green (B3)	560	10
				Red (B4)	665	10
				NIR (B8A)	865	20

4.7 Spectral characteristics of chrome mining

Chromite ore extraction is usually conducted using open cast mining. After the ore is extracted, it is then crushed, transported and processed further. It is a heavy rock, which is dark gray to black in color with a metallic to submetallic luster (Enerjigrubu.blogspot.com, 2018). Chromite ore can be described using the chemical formula: $(Fe,Mg)O.\ (Cr,Al,Fe)_2O_3$. It contains within its composition an appreciable level of iron content, and oxygen. A good grade chromite ore has a Cr_2O_3 content within the range 42–60% (or higher) and its chromium-to-iron ratio is higher than that of its lower grade equivalent (Lee, 2001). The Cr/ Fe ratio in chromite ore is important as it determines the grade of the chrome ore. Lee (2001) notes that a typical high ratio chromite ore contains 47% Cr_2O_3 minimum, and its Cr/Fe ratio will be 3,0 minimum. This means that the chromite content is an important constituent of chrome ore, and also contributes as an important constituent of one of its spectral characteristics: colour/pigmentation. The iron content can also not be discounted for its contribution to the other spectral characteristics of the chrome ore.

The chrome mining operations within this study exhibits the characteristics such as a distinct colour, size, soil pigmentation and a unique mineral composition, which renders it different from its surroundings. The size of the chrome mine workings generally ranges between 5-30m thick, depending on the methods of ore extraction and tools used. Most of the workings are open cast, with large mining machinery such as excavators used for ore extraction, whereas some are small where only small drilling equipment and hand tools are used for ore extraction, which results in a very thin linear stretch type of surface expression of the mine workings. Chrome mining operations exhibit a distinct thick-dark grey colour due to exposure of chrome ore stockpiles and a distinct liner trend, due to the nature of the surface operations, which are usually elongated along the length of the seam. Therefore, chrome mining operations can be easily detected from their surroundings. For LCC discrimination, the spectral reflectance characteristics of different LCC classes obtained from ratio combinations of spatial and spectral resolutions is essential. Spectral reflectance characteristics of the chrome mining operations (Figure 5) was used to identify its ground signature within the area and those of other different land cover classes which are represented within the study area (Figure 6) are highlighted. Other mining operations do exist in the area, and among this is the platinum mine operations with similar spectral characteristics as those of the chrome mining operations which in some instances are in close proximity to the chrome workings. Since platinum mines extract and stockpile the chrome ore, there is a possibility of signal mixing and confusion with other chrome stockpiles from open pit chrome mining operations and some artisanal, illegal chrome mining activities. Figure 7 shows a chromite occurrence anomaly map of the study area, as computed using spectral characteristics of chromite ore from the study locality.

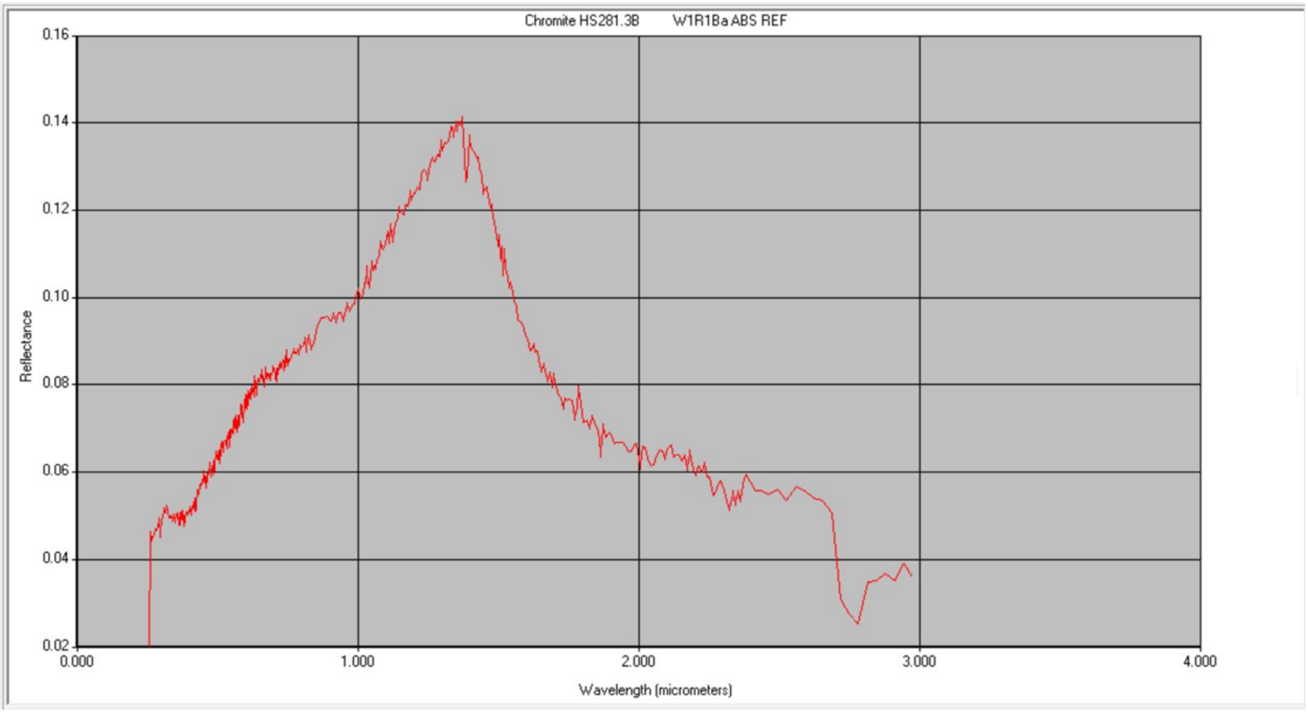

Figure 5. A computed spectral reflectance curve for the chrome mining operations found around the Atok area in Sekhukhune District, Limpopo province.

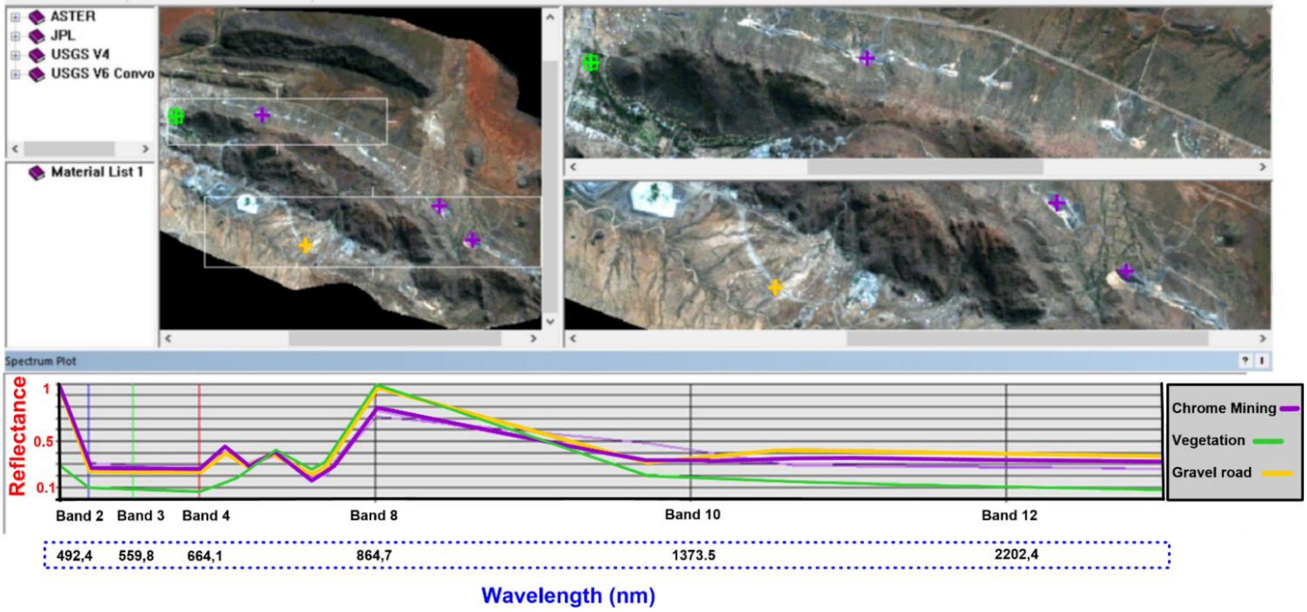

Figure 6. Spectral reflectance curves from the study area showing different land cover types. Note the differences in reflectance characteristics of different classes such as Chrome mining (in Purple), Vegetation (in Green) and Gravel roads (in Orange) and the Sentinel-2 bands selectable for discrimination of those land cover classes.

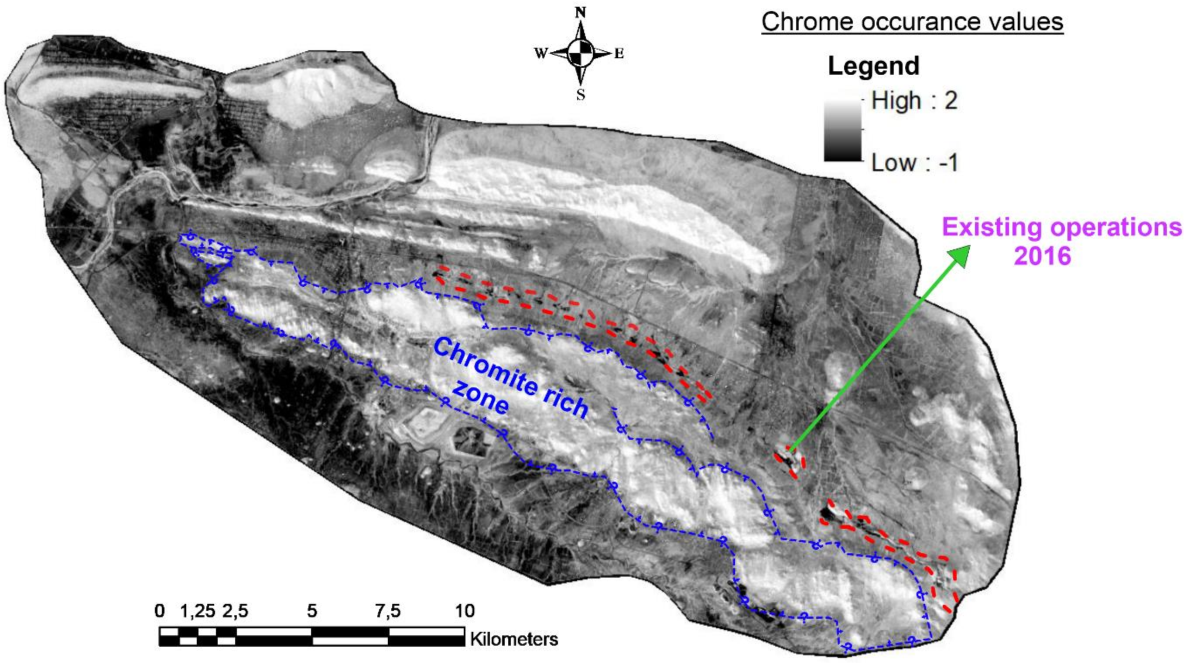

Figure 7. Chrome occurrence anomaly map of the study area, as computed from the USGS material type spectral library (USGS, 2019). This image offers an indication of the possible spatial distribution of chrome mining locations around the Atok area in Sekhukhune District, Limpopo Province, denoted by the blue outline. The red lining indicate the current workings as at 2016.

4.8 Field survey (Ground control points acquisition)

Ground truthing is a crucial step in ensuring results confirmation of classification processes. For this study, ground truthing was conducted using a total of 438 (Test data points). The land cover classes were identified using aerial imagery on Google earth and confirmed during the field visit. The bulk of the test data were acquired using a handheld GPS within the study area during November 2019, with an additional few collected using aerial imagery (Figure 8). A minimum of 30 GPS waypoints was targeted for each of the training classes. Although relatively good success was recorded in ensuring good coverage within each class, some land cover classes recorded low coverage of test data collection due to difficulties in accessing the sites or availability of roads. The same reference data was used for classification of both images. The amount of training points can be deemed adequate according to acceptable industry and academic standards for a classification study of this nature, given the dimensions of the area and number of land cover classes under assessment, to ensure reliability of the results (Lillesand *et al.*, 2015; Forkuor *et al.*, 2018). Each of the acquired waypoints was carefully selected, in order to develop a representative GCP file which included all selected training classes, for optimal validation of classification results.

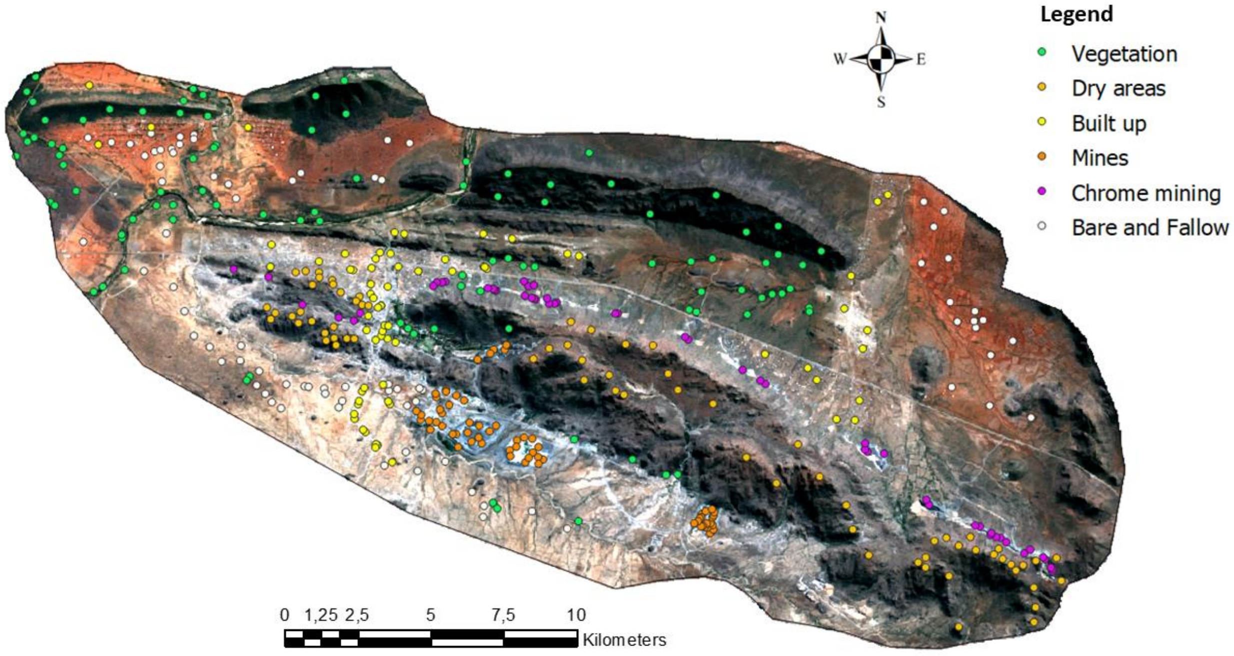

Figure 8. Image showing locations where Ground Control Points (Test data) were acquired around the Atok area in Sekhukhune District, Limpopo province.

4.9 Image classification

Image classification involves partitioning features or pixels into different classes based on the similarity of their spectral signatures (Foody, 2002). Image classification involves selection of training classes, separating pixels into various categories (clusters), assigning signals and labels to the pixels and creation of ground control points to use for feature extraction from the training classes. There are two (2) broad techniques for classification of remote sensing data, namely: unsupervised and supervised classification.

Unsupervised classification is carried out without prior knowledge of the reference data or collection of ground-truthing training dataset. Unsupervised classification involves use of an algorithm to separate groups of previously unknown pixels into different groups based on their spectral reflectance similarities. Therefore, the analyst decides how many clusters to create, and the selection of appropriate bands to use in performing the classification. Using this information, the image classification program generates clusters. A number of image clustering algorithms are in used for unsupervised classification, such as K-means, Mean-shift, ISODATA, etc.

Supervised classification involves separating data into training and testing datasets (Mather, 2004). In supervised classification, the analyst identifies the training areas which are items of a homogeneous nature that represent identical features on ground surface (Dhakal,2012) The target objects are the different surface cover types, which are grouped into different classes or training samples. “The selection of appropriate training areas is based on the analyst's familiarity with the geographical area and their knowledge of the actual surface cover types present in the image” (Dhakal 2012, p. 6). This gives the analyst control over categorisation of the selected classes. The training classes perform a task of distinguishing different land cover types on the earth`s surface within the study area. Generation of signatures to use for supervised classification is quite a tedious job, which also requires outmost accuracy to ensure that only the intended signal is picked. For the current study, care was applied to ensure that a clear discrimination of signatures is obtained, in order for the classification to generate accurate classes and minimize signal overlapping.

This study used a pixel-based image classification approach, with which all pixels are considered as belonging to a specific land cover class. In pixel-based classification, the analysis is made using only the spectral information available for each pixel. Using this approach, the classification was run with the assumption that each pixel is homogenous and belongs to a single land cover class. However, based on the spatial resolution of the imagery, the accuracy of the classification could be degraded by spectral or pixel mixing between different classes or land cover types.

Two supervised classification algorithms: The Maximum Likelihood Classifier (MLC) and Support Vector Machine (SVM) were used to quantify the changes in the land cover by identifying six spectrally different land cover classes (Table 2).

Table 2. Descriptions of major land cover classes used for the study and test data (GCPs) used for classification.

Class Name	**Description**	**Number of reference (test) data points**
Vegetation	All green vegetation (mixed), including large trees, shrubs, croplands, woodlands and broadleaf types of trees.	99
Dry areas	Dry mountainous areas largely covered by rocks with very less vegetation.	70
Built-up	All man-made infrastructure including residential units, roads, and large buildings.	70
Mines	Mine property, including the plant, large machinery (large industrial structures) and mine dumps.	68
Chrome mining	Linear and co-linear features representing open surface mining operations for chrome ore extraction.	52
Bare and fallow	All bare, fallow and exposed soils with little or no leafy vegetation.	79
Total		**438**

4.9.1 Maximum Likelihood Classifier

The maximum likelihood classifier (MLC) is parametric supervised classification algorithm widely used to classify pixels in Thematic Mapper (TM) imagery (Jia and Richards, 1994; Otukei and Blaschke, 2010). It uses a statistical estimation to derive a probability that a pixel will be assigned to a correct class in which it belongs.

For this classification, training samples were selected based on a homogenous group of image pixels, to ensure the best separability. An independent subset of test data (ground control points) was used as training samples to measure the classification accuracy levels of the MLC and SVM algorithms. Once classification is completed, a selected optimal filter known as majority filter is applied to remove isolated pixels or noise from the outputs, to refine the results. Upon completion of the classification process, a confusion matrix is computed to measure the accuracy of the results.

4.9.2 Support Vector Machine

Support Vector Machine (SVM) is a supervised machine learning that identifies a hyper-plane that is able to distinguish the input dataset into a predefined discrete number of classes consistent with training data (Rajah *et al.*, 2019). Support vectors are data points that lie closest to the decision surface (or the hyperplane). The two support hyperplanes on the boundaries of hyperplane are called support vectors having the data points on their edges and are the ones that define the optimal hyperplane (Rajah *et al.*, 2019). Its resistance to overfitting and its ability to handle even smaller samples regardless to their distribution, makes it superior over many other classifiers including the Random Forest algorithm.

A number of studies have shown that SVM has high accuracy in image classifications, especially compared to MLC classifiers (Otukei and Blaschke, 2010; Deilmai *et al.*, 2011, Bahari *et al.*, 2014). The classification performance of the SVM depends on the selection of the appropriate kernel type (Cavur *et al.*, 2019). For this study a radial basis function kernel was selected, with a maximum of 500 samples per each land cover class used for training of the classifier.

Creation of training samples (land cover classes) is based on the similarities of groups of image pixels, which ensures an improved level of class separability. Similar to the MLC classification, an independent set of test data (Ground control points) was applied to the training samples for assessing accuracy levels of the SVM classification. Once classification is completed, a selected filter known as majority filter is applied to remove isolated pixels /noise from the outputs, in order to refine the results. Once final results are obtained, classification accuracies can be determined using a confusion matrix.

4.10 Accuracy assessments

An accuracy assessment is used to assess whether individual pixels are correctly grouped within the appropriate classes of the overall sampling zone (Roy *et al.*, 2019). The accuracy assessment for this study was conducted using the training data (GPS points) acquired from the area for verification of individual land cover classes. Usually after the process of classification, images exhibit errors due to noise, weakness of classifiers and spectral confusion (Liu *et al.*, 2016). Other factors that may have an effect on the results accuracy may include landscape spatial variation and short-term inter-seasonal climate variability. An LCC accuracy assessment is conducted using statistical metrics which describes different levels of pixels accuracies within their classes. These metrics includes indicators known as the producer's accuracy, user`s accuracy, overall accuracy and the kappa coefficient. These accuracy assessment indicators are measured using the following formulas:

$$\text{Producer`s acuracy} = \frac{(\text{Total \# of correctly classified pixels in each class})}{(\text{\# of reference pixels of each class})} \times 100$$

$$\text{User`s acuracy} = \frac{(\text{Total \# of correctly classified pixels in a given class})}{(\text{Total \# of verified pixels in that class})} \times 100$$

$$\text{Overall acuracy} = \frac{\sum (\text{Total \# of correctly classified pixels in class})}{\sum (\text{Total \# of pixels of each class})} \times 100$$

The kappa coefficient:

The kappa coefficient (K) is used to evaluate agreement between the classification inputs and ground truth pixels (Mbiwa, 2018; Kraemer, 2014). A kappa value of 1 represents a state of perfect agreement between classification input entries whereas a value of 0 represents a state of no agreement. Kappa coefficient (K) is measured using the following formula:

$$K = \frac{N\sum_{i=1}^{r} X_{ii} - \sum_{i=1}^{r} X_{i+} \times X_{+i}}{\mathrm{N}^2 - \sum_{i=1}^{r} (X_{i+} \times X_{+i})}$$

Where, r = number of rows and X_{ii}= observations in row I and column i

X_{i+} and X_{+I} = the marginal totals of row I and column I respectively

N = total of observations.

4.11 Classification error consideration and correction

Classification results usually presents with errors, which are inherent in the results due to use of a particular sampling design and misclassification bias. Existence of classification errors in classifications results may result in a deviation between the classification results and the estimated true areas of change on the ground. To correct for this, it is important to calculate error adjusted land area estimates, from the constructed confusion matrix and accuracy assessment results, in order to derive accurate land cover change results. In this study, a stratified estimator is applied to determine the standard error which will be used to accurately determine the true proportions of areas of land cover changes from the classification results. This type of error adjustment was suggested by Olofsson et al. (2013) and used in a number of classification studies such as Lu et al. (2016) and Gómez (2016).The stratified estimator uses stratified random sampling points, which are used to assess the classification results, to perform a calculation of the error adjusted estimates of the mapped area of land change. A total of 500 stratified random sample points were used to assess accuracy of the classification results from each classifier. The error adjustment is made to compensate for the bias attributable to map classification results when a normal systematic sampling design is considered. This is because the systematic sampling design usually results in an overestimation of the standard error (Wolter, 2007). Therefore, the stratified sample design is used to calculate for the correct estimate of the classification error. For this study, the error adjustment is calculated with consideration of the accuracy assessment indicators, which are calculated from the confusion matrix computed for each of our classifiers i.e., MLC and SVM. The stratified estimator takes into account the omission error, which represents the reference pixels which were omitted from the correct class in a classified map. Omission error is calculated as follows:

$$\textbf{Omission error} = \left(\frac{\textbf{Incorrectly classified pixels in a given class}}{\textbf{(Total \# of verified pixels in that class)}}\right) \times 100$$

For a calculation of an unbiased error adjusted area estimates of a particular land cover class, stratified estimated values of the true proportion of the total area of the map is factored to eliminate the bias in the calculation of land cover areas, using this formula:

$$A_{\text{tot}} = W_i / A_{m_{.}i}$$

And the area of a reference class is calculated as,

$$\hat{A}_j = A_{\text{tot}} \sum W_i \frac{X_{ij}}{X_i}$$

Where, A_{tot} is the total mapped of the area study, Â is the area of a reference class, *W* is the proportion of the total area mapped in a class, *I* and *j* are the map categories (*i* =1,2,3…*q*) represented by individual land cover classes. *m* denotes that it is a mapped area. X is the marginal total of inputs in a class. Once area of a reference class is calculated, the estimated standard error of the estimated area proportion can be calculated using the following formula

$$Ś\,(\dot{P}_j) = \sqrt{\sum_{i=1}^{q} W_i{}^2 * \frac{X_i/X_{ij}\left(\frac{X_{ij}}{X_i}/\right)}{(X_i - 1)}}$$

Once the standard error is calculated, the standard error of the error adjusted estimated area can then be calculated as:

$$Ś = A_{\text{tot}} * Ś(\dot{P}_i)$$

In the above formulas, Ś is the stratified estimator, Ṗ is the proportion of the area within a class *i* or *j*. Once the stratified estimator is derived at a selected confidence level, and Ṗ is known, it can then be used to calculate the error adjusted class area sizes using the formula below.

$$A_i = A_{\text{tot}} * \dot{P}_i$$

Once the error adjusted class area sizes are known, land cover change can be calculated based on individual class changes.

4.12 Change vector analysis (CVA).

Change vector analysis is a method which is used for detection of changes in multispectral data (Fraser *et al.,* 2009). CVA is classified as one of most robust and thorough approaches for detection and in-depth characterization of radiometric change in multispectral remote sensing data (Johnson and Kasischke, 1998). It is used to highlight and identify spectral changes between two identical image scenes, which were acquired at different periods. CVA provides an output of the magnitude and direction of changes between the two images. Over the years, CVA has been widely applied in change detection studies for LULC/LCC mapping, vegetation monitoring and various other specialized remote sensing applications. For our study, a CVA was only conducted using NDVI images, to map the NDVI value changes at locations within the study area over the assessment period. The difference in NDVI values and the direction of changes were mapped to determine the local land cover change scenario. Image differencing method was utilized for highlighting the NDVI change scenario over the assessment period.

5. CHAPTER FIVE: RESULTS

Overall, land cover classification conducted during this study showed that spatial distribution of land cover classes was successfully mapped using both the MLC and SVM classifiers, with only the temporal feature changes extracted from Sentinel-2 imagery. Furthermore, the results showed that SVM classification is more accurate than MLC.

5.1 Imagery classifications: 2016 and 2019

The overall accuracy results are presented as stratified error adjusted values, based on the calculation of stratified standard error as outlined in 4.11. Generally, the SVM classifier performed slightly better than the MLC classifier. Overall producer`s accuracies for each image are summarized as averaged values based on data from both the MLC and SVM classifications. The MLC classifier achieved producer`s accuracies of 83% and 77% with kappa values of 0,77 and 0,75 for the 2016 and 2019 images respectively, while the SVM classifier achieved producer`s accuracies of 84% and 78% for 2016 and 2019 images respectively, with kappa values of 0,78 and 0,76. On the 2016 image classification, the MLC recorded  producer`s accuracies ranging between 84-94% for the chrome mining and bare soils land cover classes, similar to those obtained by the SVM classifier for the same classes (Table 3). On the 2019 image classification, both classifiers obtained accuracies above 80% for the chrome mining class, with considerable differences shown for the bare soils class, where MLC obtained producer's accuracy of 91% and whist SVM gave 94% (Table 4).

The SVM classifier achieved user`s accuracies of 92%, 76% and 91% for vegetation, built-up and chrome mining classes respectively, compared to MLC`s 84%, 73% and 91% achieved for the same land cover classes from the 2016 image. In other instances, the MLC classifier did perform better on certain individual classes than the SVM classifier. For example, for the 2016 image classification, the MLC showed user`s accuracies of 77% and 94% for built up, and bare and fallow land cover classes compared to those achieved by the SVM classifier (71% and 93%, respectively).

The resultant classified maps from the two algorithms (Figure 9) for both years indicates that dry areas (non-vegetated mountainous areas) were the most dominant land cover type around the Atok mine area. Vegetation is sparsely distributed throughout the study area, whereas chrome mining operations were mainly located in the south-western parts of the study area with some isolated occurrences in the central parts. The classified maps also show the increases in spatial distribution of the chrome mining class (purple colour) between the years 2016-2019, mainly in the southeastern portion of the area.

5.2 Accuracy Assessments

The resultant classification maps produced higher producer`s accuracies for all classes except for dry areas and built-up classes. The vegetation class attained the highest producer’s accuracy averages of all classes at 100% for 2016 and 98% for 2019 classification maps. The dry areas class obtained producer`s accuracy average of 78% and 66%, while the built-up class obtained the lowest producer`s accuracy average of 77% and 63% for the 2016 and 2019 classifications, respectively. Three other classes, vegetation, chrome mining, bare and fallow class obtained producer`s accuracy averages that were more than 80% for the two classification maps. Dry areas class obtained an average of 76% producer`s accuracy while chrome mining class obtained an average producer`s accuracy of 93% from the 2019 image.

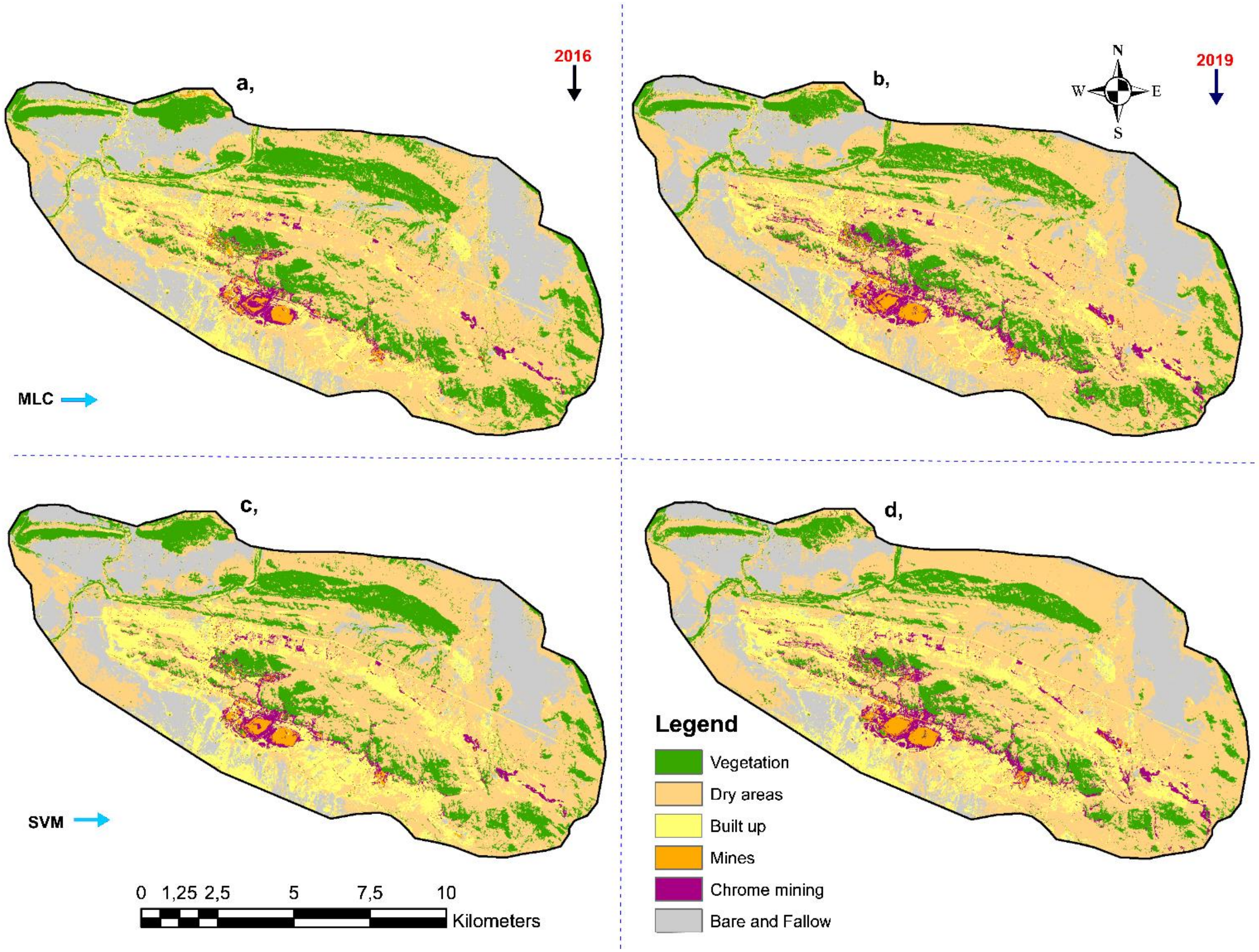

Figure 9. Classification results for land cover mapping due to expansions of chrome mining operations within the Atok area in Sekhukhune District, Limpopo province. Note the increases in spatial distribution of the chrome mining class (in purple colour) during the 4-year assessment period. The 2016 images are at the top and the 2019 images at the bottom. a, Maximum likelihood classifier(MLC) results for 2016 Sentinel-2 image, b, Maximum likelihood classifier(MLC) results for 2019 Sentinel-2 image, c, Support Vector Machine (SVM) classification results for 2016 Sentinel-2 image, and d, Support Vector Machine (SVM) classification results for 2019 Sentinel-2 image.

Table 3. Confusion matrix obtained from 2016 image of the Atok area in Sekhukhune District using Maximum Likelihood (Left) and Support Vector Machine (Right) classifiers.

2016 MLC CONFUSION MATRIX								
	VGT	DRA	BTUP	MNS	CHRM	BRF	**TOTALS**	**PA (%)**
VGT	83	0	0	0	0	0	83	**100%**
DRA	5	54	8	0	0	3	70	**77%**
BTUP	1	15	51	8	5	2	82	**62%**
MNS	8	0	6	53	1	0	68	**78%**
CHRM	2	0	0	4	49	0	55	**89%**
BRF	0	1	5	0	0	75	81	**93%**
TOTALS	99	70	70	65	55	80	**439**	
UA (%)	**84%**	**77%**	**73%**	**82%**	**89%**	**94%**		

2016 SVM CONFUSION MATRIX								
	VGT	DRA	BTUP	MNS	CHRM	BRF	**TOTALS**	**PA (%)**
VGT	91	0	0	0	0	0	91	**100%**
DRA	6	50	5	0	0	2	63	**79%**
BTUP	0	20	53	9	2	3	87	**61%**
MNS	0	0	6	54	3	1	64	**84%**
CHRM	2	0	1	2	50	0	55	**91%**
BRF	0	0	5	0	0	74	79	**94%**
TOTALS	99	70	70	65	55	80	**439**	
UA (%)	**92%**	**71%**	**76%**	**83%**	**91%**	**93%**		

Overall Acuracy: **83%**

Stratified standard error: **0.025**

Stratified error adjusted Overall Acuracy: **83%**

Kappa: **0,77**

Overall Acuracy: **84.5%**

Stratified standard error: **0.107**

Stratified error adjusted Overall Acuracy: **84%**

Kappa: **0,78**

Notes : UA= User`s acuracy, PA= Producer`s acuracy.

VGT= Vegetation; DRA= Dry areas; BTUP= Built-up; MNS=Mines;

CHRM= Chrome mining; BRF= Bare and fallow

Table 4. Confusion matrix obtained from 2019 image of the Atok area in Sekhukhune District using Maximum Likelihood (Left) and Support Vector Machine (Right) classifiers.

2019 MLC CONFUSION MATRIX

	VGT	DRA	BTUP	MNS	CHRM	BRF	**TOTALS**	**PA (%)**
VGT	72	2	0	0	0	0	74	**97%**
DRA	15	56	11	0	0	4	86	**65%**
BTUP	0	12	48	11	3	3	77	**62%**
MNS	5	0	5	50	0	0	60	**83%**
CHRM	6	0	0	4	52	0	62	**84%**
BRF	1	0	6	0	0	73	80	**91%**
TOTALS	99	70	70	65	55	80	**439**	
UA (%)	**73%**	**80%**	**69%**	**77%**	**95%**	**91%**		

2019 SVM CONFUSION MATRIX

	VGT	DRA	BTUP	MNS	CHRM	BRF	**TOTALS**	**PA (%)**
VGT	72	0	0	0	1	0	73	**99%**
DRA	18	53	7	0	0	1	79	**67%**
BTUP	1	17	56	7	3	4	88	**64%**
MNS	2	0	4	54	2	2	64	**84%**
CHRM	4	0	0	4	49	0	57	**86%**
BRF	2	0	3	0	0	73	78	**94%**
TOTALS	99	70	70	65	55	80	**439**	
UA (%)	**73%**	**76%**	**80%**	**83%**	**89%**	**91%**		

Overall Acuracy: **80%**

Stratified standard error: **0.117**

Stratified error adjusted Overall Acuracy: **77%**

Kappa: **0,75**

Overall Acuracy: **81%**

Stratified standard error: **0.119**

Stratified error adjusted Overall Acuracy: **78%**

Kappa: **0,76**

Notes : UA= User`s acuracy, PA= Producer`s acuracy.

VGT= Vegetation; DRA= Dry areas; BTUP= Built-up; MNS=Mines;

CHRM= Chrome mining; BRF= Bare and fallow

5.3 NDVI results

The NDVI results showed high values over the densely vegetated areas in the northwestern and the eastern portions of the area. Areas with extremely high NDVI values (shown in bright green) represents parts of the study area with considerable amounts of green and healthy leafy vegetation (Figure 10a, and b). The low vegetated or dry areas are represented in yellow or brown shading on both images. The low NDVI values are noted in the areas with a large number of man-made infrastructure such as residential/built up sites, mines and new chrome mining operations The 2019 NDVI image exhibits more areas with extremely low NDVI values than the 2016 image. This is indicated by the reddish-brown shading on in the southeastern tip of the map (Figure 11a, and b). Note the increase in surface area of the extreme low NDVI locations on the 2019 image. An image differencing method was used to determine the change scenario between the 2016 and 2019 NDVI results. Change Vector Analysis results (Figure 11) were able to highlight the change in exposed lands due development of new chrome mining operations in the southeastern portion of the study area, where most of the chrome mining activities occurs within the study area, including illegal and artisanal miner`s operation.

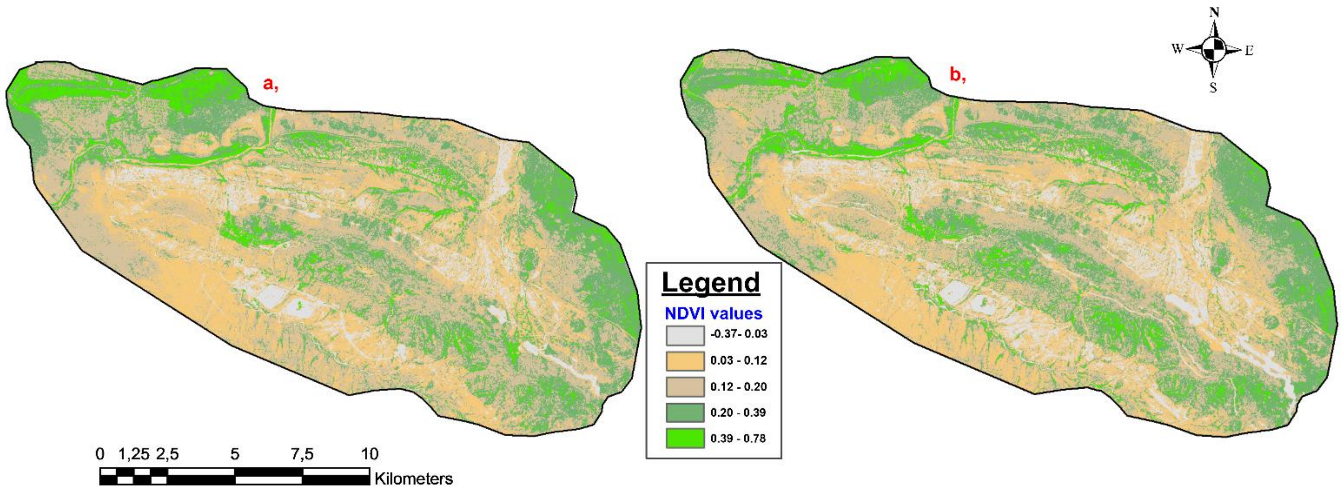

Figure 10. The normalized difference vegetation index (NDVI) results used for land cover mapping due to expansions of chrome mining operations within the Atok area in Sekhukhune District, Limpopo province. a, The 2016 NDVI results image. b, The 2019 NDVI results image, note the increases in extreme low values (whitish-grey) on regions where bare soil exposure is high, including mine dumps and new chrome mining operations, around the south-eastern corner of the image.

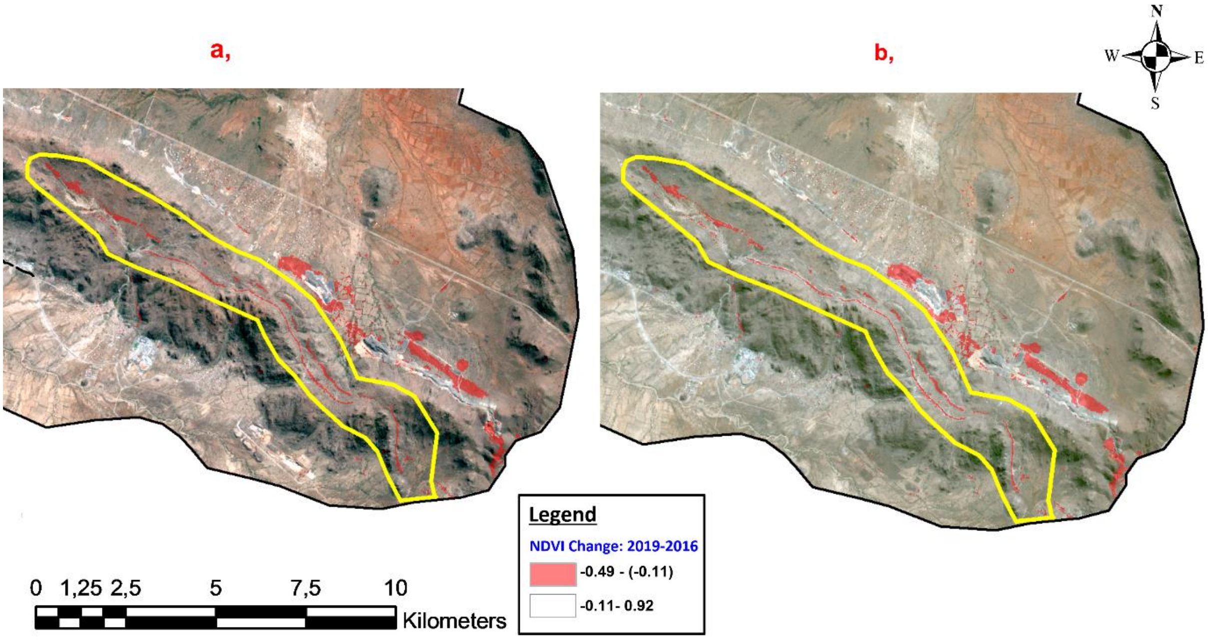

Figure 11. An extract of zoomed NDVI results used for land cover mapping due to expansions of chrome mining operations within the Atok area in Sekhukhune District, Limpopo province. a, shows an area of high NDVI change in extreme low NDVI values the 2016 image, shown by the reddish trace. b, shows an area of high NDVI change in extreme low NDVI values on the 2019 image. Note the traces of low NDVI values following locations where newer chrome mining operations are visible (light whitish-grey traces within the yellow outline). The 2016 image has fewer or shorter whitish-greyish traces (workings) than the 2019 image

5.4 Quantification of land cover change 2016-2019

The LCC results are presented herein as stratified error adjusted averaged values from the two classifiers. The results show that in 2016 there was on average 17,2% vegetation cover, but after four years vegetation cover has decreased to a 13.8% average (Table 5). Overall, vegetation cover has decreased by an average of 3,3%, which represents a decrease of 648,6 hectares over the study area during the four-year period. Of great significance to mention in this study, is that during the same period, chrome mining class increased from 2,3% average in 2016 to 3,9% average in 2019. This represents an overall 1,6% average increase (Figure 12) which translates to an increase of 314,5 hectares over the four years period. This increase means that over 314.5 hectares of surface land has been converted from other land cover classes to new chrome mining operations than it was in 2016. Dry areas class also increased over the assessment period, from a 46,1% average to a 50% average, which gives an overall growth of 3,9%, which translates to an increase of 766,5 hectares of newly exposed non-vegetated or bare lands. Bare and fallow class decreased from 19,5% to an 18.2% average during the assessment period.

Table 5 below details spatial distribution and area statistics of the six land cover classes and the land cover class transformations that occurred within the study area, as measured using changes in area coverage by an individual land cover class during the assessment period.

Table 5. Distribution of land classes around the Atok mine area in terms of area sizes (hectares) and expressed as a percentage during the assessment period.

Land Cover Class	**Land cover 2016**				**Land cover 2019**			
	MLC 2016		**SVM 2016**		**MLC 2019**		**SVM 2019**	
	Area (ha)	% of land	Area (ha)	% of land	Area (ha)	% of land	Area (ha)	% of land
Vegetation	3680.1	18.7%	3103.8	15.8%	3023.3	15.4%	2415.4	12.3%
Dry areas	9124.0	46.4%	8999.8	45.8%	9803.6	49.9%	9824.6	50.0%
Built-up	2245.4	11.4%	3203.5	16.3%	2102.9	10.7%	2965.7	15.1%
Mines	280.1	1.4%	155.8	0.8%	291.5	1.5%	214.2	1.1%
Chrome mining	456.9	2.3%	450.6	2.3%	743.5	3.8%	784.2	4.0%
Bare and fallow	3896.2	19.8%	3752.4	19.1%	3691.5	18.8%	3478.6	17.7%
Totals	19653.2	100.0%	19653.2	100.0%	19653.1	100.0%	19653.2	100.0%

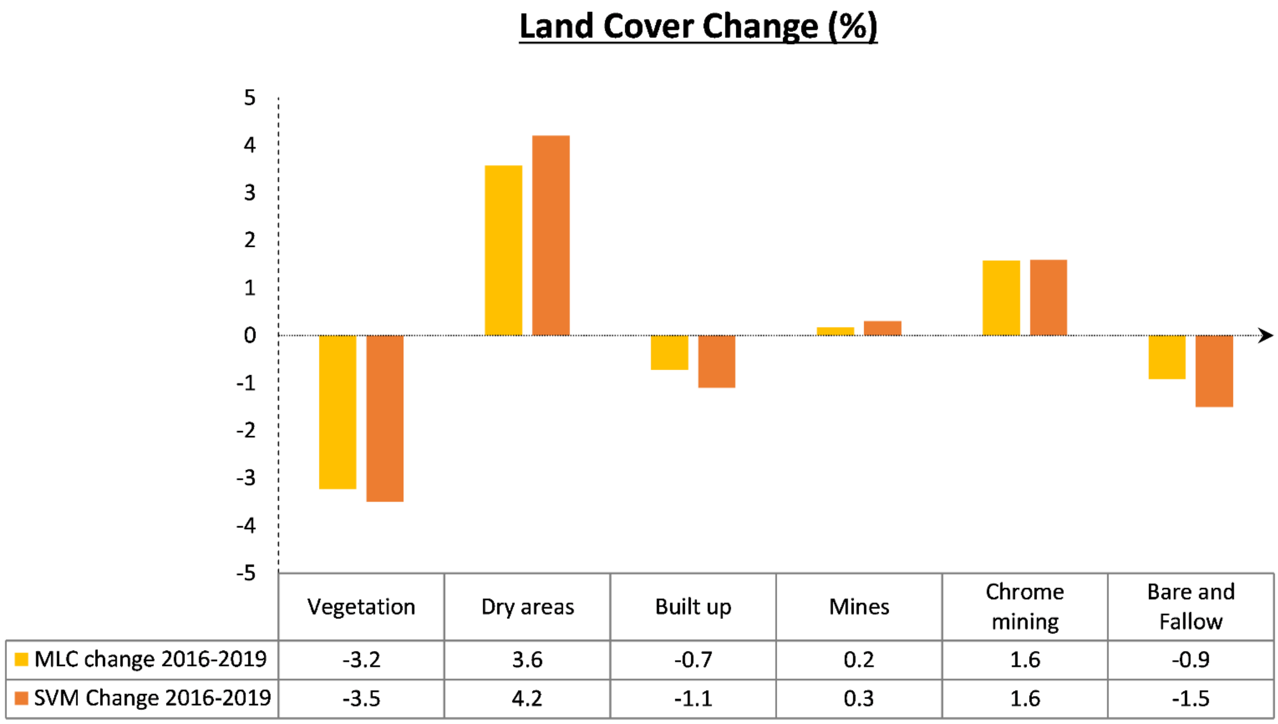

Figure 12. Percentage area change of the land cover classes during the period 2016-2019 within the Atok area in Sekhukhune District, Limpopo province. There has been a decrease in vegetation, built-up, bare and fallow classes, while the dry areas and chrome mining classes experienced gains during the 4 year period under assessment.

6. CHAPTER SIX: DISCUSSION

6.1 Analysis of study results

The main aim of the study were to make use of MLC and SVM supervised classification techniques, to identify and quantify land cover change that occurred in the Atok area due to expansion of chrome mining activities over a period of four years. The two classification algorithms used successfully identified and quantified areas of major land cover changes as affected by an increase in spatial distribution of surface mining operations. Both algorithms produced satisfactory results although the SVM classifier performed better than the MLC algorithm. The overall accuracy differences were marginal, with 1,5% obtained for the 2016 image and 1% performance difference obtained for the 2019 image classification results.

6.2 Analysis of accuracy assessments

In general, satisfactory overall classification accuracies (between 80-85%) were obtained for both the 2016 and 2019 images. The highest overall accuracy was recorded on the 2016 image classification using the SVM classifier (84,5%) and the lowest recorded overall accuracy (81 %) was obtained on the 2019 using MLC. As evidenced in LCC or LULC studies such as those conducted by Forkuor et al. (2018) and Waylen et al. (2014), overall classification accuracies around 60-80% can be considered acceptable for areas of extreme complexity where high levels of signal mixing and confusions were expected, as was the case in this study.

Classification results also showed some spectral confusion and pixel mix-ups, particularly between the dry areas and the bare and fallow classes. Most of the spectral confusion between the two classes was due to similarities in spectral signatures of the two classes and a lack of uniformity in surface expression of bare soils within the area. As a result of the spectral confusion, these two classes produced the lowest averages of producer`s accuracies from the two classifiers, with dry areas class obtaining 78% and 66% while the bare and fallow class obtained 61,5% and 63% for the 2016 and 2019 images respectively. Some of the spectral confusion was mapped to come from chrome mining class, due to chrome ore residue contamination in the soils of the areas near the mining operations, which also affected the bare and fallow class. The chrome ore contamination was found to happen due to chrome ore stockpiling within some villages, spillages, during transportation, or as a result of artisanal and illegal mining activities, while some were due to storage of chrome ore residue in large PGM mine tailings dams. The two classifiers managed to separate man-made infrastructure such as residential units and mine infrastructure from the other land cover types such as chrome mining operations and dry areas effectively.

Overall, the results obtained in this study are consistent with those found in literature. For instance, the overall accuracies obtained for the SVM algorithm in this study are similar to those archived in the study by Jiang et al. (2011), which analyzed the potential of SVM, ANN and decision tress for mapping the change in forest cover within the Guangdong Province of China. Their classifications achieved overall accuracies above 88% for the SVM classifier, as well as the ANN and decisions trees. In a study similar to the current one, Deilmai et al. (2011) conducted a study focusing on land cover change classification and monitoring of land use changes, where they compared classification results from the SVM and MLC algorithms. Their results showed that SVM produced slightly better results than MLC, with an overall accuracy of 91,67% and a kappa coefficient of 0.86 for SVM and 78,33% with a kappa coefficient of 0,65 for the MLC.

6.3 NDVI analysis of results

Change Vector Analysis (CVA) results indicated a positive change in NDVI results for the 2016 to 2019 images. Image differencing method identified the changes NDVI values on specific locations, which helped in highlighting growth in the chrome mining operations around the area and corresponded well with land cover change scenarios as mapped using the two classification algorithms. There were distinct changes in the low NDVI values (≤ -0,1) over areas where new mining operations exists, and subtle changes in the high NDVI values (≥ 0,1) over the highly vegetated areas of the north-western portion of the area. Trend analysis on the NDVI images clearly indicate a continuity in the extreme low NDVI values (-0,1 to -1) over areas where expansions of chrome mining operations exists and new exposures of bare soils/non-vegetated areas. Overall, the NDVI results managed to highlight areas of vegetation loss/bare soil changes within the whole of the study area.

6.4 Impacts on local land cover change

Generally, mining activities impact do affect the local environments severely (Kumi-Boateng *et al.*, 2012). The size and type of operations ran usually determines the levels of environmental impacts created by the mine. Open cast mining in particular results in significant pollution of local environments and usually leads to severe degradation of the ecological and aesthetic quality of a landscape. Disruption of the surface due to mining works severely affects soils, plants, animals, local water channels and small living organisms, thereby influencing all types of land use (Özyavuz, 2013). Quantification and analysis of Land cover change (LCC) is important for evaluating impacts of mining on landscape degradation and local environmental pollution around rural settlements. As evidenced in the study Petit et al. (2001) Land cover change(LCC) studies can be used useful in determining the direction of major changes and spatio-temporal patterns of change, quantifying percentages of areas affected and rates of change, mapping/quantification of impacts on natural vegetation and prediction of future spatial distributions in land-cover. Results from this study show that the land cover changes mapped within the study area are two dimensional: (1) quantitative changes in area occupied by each land cover class, (which are recorded as losses or gains per class) and (2) the spatial transformations of land cover classes/types.

The analysis of the change statistics from the two classification outputs indicate that some land cover classes increased over the assessment period while others shrank. In particular, increases were observed for chrome mines, and dry areas, whereas the surface areas occupied by vegetation, bare and fallow areas decreased. The losses in percentage cover by vegetation means a considerable number of trees were cleared to make way for the new mining operations. The moderate increase in dry areas class is a result of new exposures via stripping and open cast mining in the new chrome mining operations. Similar occurrence was experienced in the study by Ololade et al. (2008). This shows that some of the newer chrome mining operations have been developed on lands previously classified as bare and fallow. These land cover transformations may have severe impacts on soil erosion (Matsika, 2007 and Ngcofe *et al.*, 2019), soil contamination and hydrological processes such as seepage or run-off (Cao *et al.*, 2009 and Gordon *et al., 2005*), water quality, the sustainability of the local environment (Lupo *et al*., 2001) and a may lead to major alterations in local ecological dynamics.

A good agreement between the gains recorded by chrome mining class, dry areas class and the losses incurred by the vegetation class is observed, solidifying the reliability of temporal land cover change mapping as a good indicator for understanding the intra-relationships between transformed land cover classes within an environment. As stated before, some of the chrome mining operations within the study area are conducted by small-scale and illegal miners. Similarly, Tom-Dery et al. (2012) found that activities of artisanal miners in Ghana had a capacity to severely affect the numbers of shrubs and tree species through illegal clearing of vegetation, thereby impacting on the local plant diversity in an area. These land cover changes could also be used for prediction of possible future footprints of chrome mining expansions in the area. It would be important for authorities to ensure that once extraction of the chrome ore resources is over, mining companies are held liable to make sure that restoration and reclamation of the altered landscape is conducted.

7. CHAPTER SEVEN: CONCLUSIONS

The main findings of this study are that both the maximum likelihood classifier and support vector machines classifiers managed to successfully map and quantify land cover changes due to expansions of chrome mining operations over the four-year assessment period. Sentinel-2 imagery has proven to be adequate for land cover change due to chrome mining operations, indicating its impacts on the natural vegetation at the environment around the study area. Results from this study highlighted the progressive expansion of the chrome mining operations in the area, including operations conducted by small-scale miners as well as areas where chrome mining is suspected to be conducted illegally. Classification results exhibited the variation in spatial distribution of land cover types within the area, their diversity and the intra-class transformations that occurred over the assessment period. Using the results statistics, it became possible to identify areas of rapid change and evaluate the current conditions and the quantities of different land cover types within the area. This measurement offers a better understanding of the change dynamics, development trends and possible future impacts. More importantly, the study managed to highlight the effect which chrome mining operations has on other land cover classes within the study area, as well as highlighting the environmental impacts thereof. Some of the main study findings includes:

- Overall, the use of Sentinel-2 imagery coupled with other ancillary data proved to be useful for identification and quantification of land cover change (LCC) within the Atok area over the period 2016-2019
- Comparison of MLC and SVM classification algorithms showed that the SVM classifier slightly outperformed the MLC by a margin of 1% for both the 2016 and the 2019 images.
- The MLC classifier achieved 83% and 80% stratified error adjusted overall accuracies with kappa values of 0,77 and 0,75 for the 2016 and 2019 images respectively, while the SVM classifier achieved stratified error adjusted overall accuracies of 84% and 78% for 2016 and 2019 images respectively, with kappa values of 0,78 and 0,76.
- Classification results highlighted a substantial decreases in the total area coverage of green vegetation, shrubs, and woodlands, especially in the mountainous areas, which is attributed to an increase in the total area coverage of bare soils and expansions of chrome mining operations during the measured four (4) year period

- Chrome mining class accounted for approximately 2,3% of land cover in the year 2016, and now constitutes a 3,9% of the land cover within the study area in 2019.
- Over 314,5 hectares of surface land within the study area has been transformed from other land cover classes to new chrome mining operations during the period 2016-2019.
- There has also been a transformation of about 766,5 hectares to newly exposed dry areas within the Atok area during the assessment period.
- This study shows a clear growth trend in development of chrome mining operations in the area, which is expected to continue into the near future.
- The major transformations in land cover recorded over the four (4) year period has contributed to a decrease in landscape quality, decrease in vegetation growth and an increase in the levels of landscape deterioration and overall environmental pollution within the study area.

The inclusion of the vegetation index (NDVI) provided additional information useful for the discrimination between green vegetated slopes and dry areas. NDVI results contributed to high-lighting of new areas of dry soil exposures, which are attributable to development of new chrome mining operations. NDVI also proved to be a sufficient indicator of distribution for both presence and the depletion of green leafy vegetation over the landscape, which was found to be severely impacted by clearing of trees, for development of new mining sites. Use of ground control points provided important test data for use in evaluation of land cover changes over the area. The use of combined results of MLC and SVM classification algorithms, as well as NDVI data has proved useful for mapping of the chrome mining development around the Atok area, and offers insights into future prospects for environmental monitoring of impacts from the mining operations on the landscape and local ecosystems.

8. REFERENCES

Ackerman, E.R., 2011. *Sequential land cover classification*. MSc Dissertation, Pretoria, University of Pretoria.

Adam, E., Mutanga, O., Odindi, J. and Abdel-Rahman, E.M., 2014. Land-use/cover classification in a heterogeneous coastal landscape using RapidEye imagery: Evaluating the performance of random forest and support vector machines classifiers. *International Journal of Remote Sensing*, *35*(10), pp.3440-3458.

Africa Mining IQ. 2019. Chrome mining in South Africa. [Online]: Available at: https://www.projectsiq.co.za/chrome mining-in-south-africa.htm. [Accessed 12 July 2019].

Bahari, N.I.S., Ahmad, A. and Aboobaider, B.M., 2014. Application of support vector machine for classification of multispectral data. In *IOP Conference Series: Earth and Environmental Science* (Vol. 20, No. 1, p. 012038). IOP Publishing.

Cao, W., Bowden, W.B., Davie, T. and Fenemor, A., 2009. Modelling impacts of land cover change on critical water resources in the Motueka River catchment, New Zealand. *Water Resources Management*, *23*(1), pp.137-151.

Cavur, M., Duzgun, H.S., Kemec, S. and Demirkan, D.C., 2019. Land use and land cover classification of Sentinel 2-A: St Petersburg case study. *International Archives of the Photogrammetry, Remote Sensing & Spatial Information Sciences*.

Chatziantoniou, A., Psomiadis, E. and Petropoulos, G.P., 2017. Co-orbital Sentinel 1 and 2 for LULC mapping with emphasis on wetlands in a mediterranean setting based on machine learning. *Remote Sensing*, *9*(12), p.1259.

Clerici, N., Valbuena Calderón, C.A. and Posada, J.M., 2017. Fusion of Sentinel-1A and Sentinel-2A data for land cover mapping: A case study in the lower Magdalena region, Colombia. *Journal of Maps*, *13*(2), pp.718-726.

Chander, G., Markham, B.L. and Helder, D.L., 2009. Summary of current radiometric calibration coefficients for Landsat MSS, TM, ETM+, and EO-1 ALI sensors. *Remote Sensing of Environment*, *113*(5), pp.893-903.

Coetzee, J.J., Bansal, N. and Chirwa, E.M., 2020. Chromium in environment, its toxic effect from chromite-mining and ferrochrome industries, and its possible bioremediation. *Exposure and Health*, *12*(1), pp.51-62.

Deilmai, B.R., Ahmad, B.B. and Zabihi, H., 2014. Comparison of two classification methods (MLC and SVM) to extract land use and land cover in Johor Malaysia. In *IOP Conference Series: Earth and Environmental Science* (Vol. 20, No. 1, p. 012052). IOP Publishing.

Department of Environmental Affairs (DEA). 2016. Land cover map 2015. [Online]: Available at: https://egis.environment.gov.za/data_egis/data_download/current. [Accessed 26 June 2019].

Department of Environmental Affairs (DEA). 2019. Land cover map 2018. [Online]: Available at: https://egis.environment.gov.za/data_egis/data_download/current. [Accessed 26 June 2019].

Dhakal, S., 2012. Land cover change and urban settlement extraction in Kathmandu Valley using Remote Sensing: A Proposition. *GeoSpace, Journal of Geomatics Engineering Society, Kathmandu University: V0l 1.*

Dlamini, S. N., Beloconi, A., Mabaso, S., Vounatsou, P., Impouma, B., and Fall, I. S., 2019. Review of remotely sensed data products for disease mapping and epidemiology. *Remote Sensing Applications.* 14, 108–118. doi: 10.1016/j.rsase.2019.02.005

Drusch, M., Del Bello, U., Carlier, S., Colin, O., Fernandez, V., Gascon, F., Hoersch, B., Isola, C., Laberinti, P., Martimort, P. and Meygret, A., 2012. Sentinel-2: ESA's optical high-resolution mission for GMES operational services. *Remote Sensing of Environment*, *120*, pp.25-36.

Eales, H.V. and Cawthorn, R.G., 1996. The Bushveld complex. In: Cawthorn, R. G. (ed.) *Layered Intrusions.* Amsterdam: Elsevier, pp. 181–232.

Earth Lab. 2019. Lesson 4. Calculate NDVI in R: Remote sensing vegetation index. [Online]: Available at: https://www.earthdatascience.org/courses/earth-analytics/multispectral-remote-sensing-data/vegetation-indices-NDVI-in-R/. [Accessed 26 February 2020]

Emetere, M.E., 2019. Image reprocessing of satellite imageries. In *Environmental modeling using satellite imaging and dataset re-processing.* Studies in Big Data, vol 54. Springer publishing.

Engineering News. 2019. Chrome ore exports contribute to stainless steel production. [Online]: Available at: https://m.engineeringnews.co.za/article/s-africa-chrome-ore-exports-contribute-to-stainless-steel-production-2019-05-15/rep_id:4433. [Accessed 26 Febraury 2020]

European Space Agency (ESA). 2016. Sentinel-2 MSI spatial resolution. [Online]: Available at: https://earth.esa.int/web/Sentinel-2/user-guides/Sentinel-2-msi/resolutions/spatial. [Accessed 21 July 2019].

Fichera, C.R., Modica, G., and Pollino, M., 2012. Land Cover classification and change-detection analysis using multi-temporal remote sensed imagery and landscape metrics. *European Journal of Remote Sensing*, 45(1), pp.1-18.

Fogg, C.T. and Cornellisson, J.L., 1993. *Availability of platinum and platinum-group metals* (Vol. 9338). US Department of the Interior, Bureau of Mines, Washington, pp. 54.

Foody, G.M., 2002. Status of land cover classification accuracy assessment. *Remote Sensing of Environment*, *80*(1), pp.185-201.

Forkuor, G., Dimobe, K., Serme, I. and Tondoh, J.E., 2018. Landsat-8 vs. Sentinel-2: examining the added value of Sentinel-2's red-edge bands to land-use and land-cover mapping in Burkina Faso. *GIScience and remote sensing*, *55*(3), pp.331-354.

Fraser, R.H., Olthof, I. and Pouliot, D., 2009. Monitoring land cover change and ecological integrity in Canada's national parks. *Remote Sensing of Environment*, *113*(7), pp.1397-1409.

Giri, C.P., 2016. Remote sensing of land use and land cover: Principles and applications. CRC press, Boca Raton, FL, USA, pp. 477.

Gómez, C., White, J.C. and Wulder, M.A., 2016. Optical remotely sensed time series data for land cover classification: A review. *ISPRS Journal of Photogrammetry and Remote Sensing*, *116*, pp.55-72.

Gordon, L.J., Steffen, W., Jönsson, B.F., Folke, C., Falkenmark, M. and Johannessen, Å., 2005. Human modification of global water vapor flows from the land surface. *Proceedings of the National Academy of Sciences*, *102*(21), pp.7612-7617.

Hassan, Z., Shabbir, R., Ahmad, S.S., Malik, A.H., Aziz, N., Butt, A. and Erum, S., 2016. Dynamics of land use and land cover change (LULCC) using geospatial techniques: A case study of Islamabad Pakistan. SpringerPlus, 5(1), pp.812.

Herrmann, S. M., Anyamba, A., and Tucker, C.J., 2005. Recent trends in vegetation dynamics in the African Sahel and their relationship to climate. *Global Environmental Change* 15,394-404.

InvestSA. 2020. Fact sheet: mining, 2020. [Online]: http://www.investsa.gov.za/wp-content/uploads/2020/02/fact-sheet_mining_2020.pdf [Accessed: 06 October 2020].

Jia, X. and Richards, J.A., 1994. Efficient maximum likelihood classifier for imaging spectrometer data sets. *IEEE Transactions on Geoscience and Remote Sensing*, *32*(2), pp.274-281.

Jiang, X., Lin, M. and Zhao, J., 2011. Woodland cover change assessment using decision trees, support vector machines and artificial neural networks classification algorithms. In *Fourth International Conference on Intelligent Computation Technology and Automation* (Vol. 2, pp.312-315). IEEE *2011*, Washington DC, United States.

Johnson, R.D. and Kasischke, E.S., 1998. Change vector analysis: A technique for the multispectral monitoring of land cover and condition. *International Journal of Remote Sensing*, *19*(3), pp.411-426.

Kraemer, H.C., 2014. Kappa coefficient. *Wiley StatsRef: Statistics Reference Online*, pp.1-4.

Kumi-Boateng, B., Mireku-Gyimah, D. and Duker, A.A., 2012. A spatio-temporal based estimation of vegetation changes in the Tarkwa mining area of Ghana. *Research Journal of Environmental and Earth Sciences,* 4(3), pp 215-229.

Lee, Y.E., 2001. Ferroalloys: Production and use in Steel-making. *Encyclopedia of Materials: Science and Technology (Second Edition),* pp.3039-3044.

Lee, C.A. and Parry, S.J., 1988. Platinum-group element geochemistry of the lower and middle group chromitites of the eastern Bushveld complex. *Economic Geology*, *83*(6), pp.1127-1139.

Lillesand, T., Kiefer, R.W. and Chipman, J., 2015. *Remote sensing and image interpretation*. John Wiley and Sons.

Lu, D. and Weng, Q., 2007. A survey of image classification methods and techniques for improving classification performance. *International Journal of Remote Sensing*, *28*(5), pp.823-870.

Lu, D., Chen, Q., Wang, G., Liu, L., Li, G. and Moran, E., 2016. A survey of remote sensing-based aboveground biomass estimation methods in forest ecosystems. *International Journal of Digital Earth*, *9*(1), pp.63-105.

Liu, M., Cao, X., Li, Y., Chen, J. and Chen, X., 2016. Method for land cover classification accuracy assessment considering edges. *Science China Earth Sciences*, *59*(12), pp.2318-2327.

Lupo, F., Reginster, I. and Lambin, E.F., 2001. Monitoring land-cover changes in West Africa with SPOT Vegetation: Impact of natural disasters in 1998-1999. *International Journal of Remote Sensing*, *22*(13), pp.2633-2639.

Enerjigrubu.blogspot.com. (2018). Chromite. [Online]: http://enerjigrubu.blogspot.com/2018/09/chromite-only-ore-of-chromium-metal.html. [Accessed: 29 August 2019].

Özyavuz, M., 2013. Inventory and analysis of the landscape. In *Advances in Landscape Architecture*. IntechOpen, Rijeka, Croatia, pp.339.

Makaya, N.P., Mutanga, O., Kiala, Z., Dube, T. and Seutloali, K.E., 2019. Assessing the potential of Sentinel-2 MSI sensor in detecting and mapping the spatial distribution of gullies in a communal grazing landscape. *Physics and Chemistry of the Earth, Parts A/B/C*, *112*, pp.66-74.

Mashamba, T., 2017. Mapping grass nutrient phosphorus (P) and sodium (NA) across different grass communities using Sentinel-2 data. MSc dissertation, University of the Witwatersrand, Johannesburg, South Africa.

Mather, P.M., 2004. Computer processing of remotely-sensed images. 3rd Ed. University of Nottingham, England.

Matsika, R., 2007. Land-cover change: Threats to the grassland biome of South Africa. PhD dissertation, University of the Witwatersrand, Johannesburg, South Africa.

Mavunda, A.N., 2016. The effects of chrome mining activities on the water quality of the Hex River in the Rustenburg area: case study on Kroondal chrome mine. MSc research report, University of the Witwatersrand, Johannesburg, South Africa.

Mbiwa, L.N., 2018. Analysis of land cover changes of the Hartebeesthoek Radio Astronomy Observatory environment over five decades. MSc dissertation, University of Pretoria, Pretoria, South Africa.

McLaren, C.H. and De Villiers, J.P., 1982. The platinum-group chemistry and mineralogy of the UG-2 chromitite layer of the Bushveld Complex. *Economic Geology*, *77*(6), pp.1348-1366.

Melesse, A.M. and Abtew, W. ed., 2016. *Landscape dynamics, soils and hydrological processes in varied climates* (pp. 1-93). New York, NY: Springer International Publishing.

Mensah, A.K., Mahiri, I.O., Owusu, O., Mireku, O.D., Wireko, I. and Kissi, E.A., 2015. Environmental impacts of mining: a study of mining communities in Ghana. *Applied Ecology and Environmental Sciences*, *3*(3), pp.81-94.

Mpandeli, S., Nesamvuni, E. and Maponya, P., 2015. Adapting to the impacts of drought by smallholder farmers in Sekhukhune District in Limpopo province, South Africa. *Journal of Agricultural Science*, *7*(2), p.1-15.

Münch, Z., Okoye, P.I., Gibson, L., Mantel, S. and Palmer, A., 2017. Characterizing degradation gradients through land cover change analysis in rural Eastern Cape, South Africa. *Geosciences*, *7*(1), p.7.

Mundia, C.N. and Aniya, M., 2005. Analysis of land use/cover changes and urban expansion of Nairobi city using remote sensing and GIS. *International journal of Remote sensing*, *26*(13), pp.2831-2849.

Nagendra, H., Reyers, B. and Lavorel, S., 2013. Impacts of land change on biodiversity: Making the link to ecosystem services. *Current Opinion in Environmental Sustainability*, *5*(5), pp.503-508.

Ngcofe, L. and Thompson, M., 2015. The status of land cover mapping in South Africa: 1994-2015.

Ngcofe, L.D., Hickson, R. and Singh, P., 2019. The South African land cover change detection derived from 2013_2014 and 2017_2018 land cover products. *South African Journal of Geomatics*, *8*(2), pp.160-177.

Olofsson, P., Foody, G.M., Stehman, S.V. and Woodcock, C.E., 2013. Making better use of accuracy data in land change studies: Estimating accuracy and area and quantifying uncertainty using stratified estimation. *Remote Sensing of Environment*, *129*, pp.122-131.

Ololade, O., Annegarn, H.J., Limpitlaw, D. and Kneen, M.A., 2008. Land-use/cover mapping and change detection in the Rustenburg Mining Region using Landsat images. In *IGARSS 2008-2008 IEEE International Geoscience and Remote Sensing Symposium* (Vol. 4, pp. IV-818). IEEE.

Otukei, J.R. and Blaschke, T., 2010. Land cover change assessment using decision trees, support vector machines and maximum likelihood classifier algorithms. *International Journal of Applied Earth Observation and Geoinformation*, 12, pp. S27-S31.

Petit, C., Scudder, T. and Lambin, E., 2001. Quantifying processes of land-cover change by remote sensing: resettlement and rapid land-cover changes in south-eastern Zambia. *International Journal of Remote Sensing*, *22*(17), pp.3435-3456.

Phiri, D., Simwanda, M., Salekin, S., R Nyirenda, V., Murayama, Y. and Ranagalage, M., 2020. Sentinel-2 data for land cover/use mapping: A review. *Remote Sensing*, *12*(14), p.2291.

Rajah, P., Odindi, J., Mutanga, O. and Kiala, Z., 2019. The utility of Sentinel-2 vegetation indices (VIs) and Sentinel-1 Synthetic Aperture Radar (SAR) for invasive alien species detection and mapping. *Nature Conservation*, *35*, p.41.

Rimal, B., Rijal, S. and Kunwar, R., 2020. Comparing support vector machines and maximum likelihood classifiers for mapping of urbanization. *Journal of the Indian Society of Remote Sensing*, *48*(1), pp.71-79.

Roy, S., Singh, N., Kumar, P., Kimothi, M.M. and Mamatha, S., 2019. Inventory and assessment of coriander crop in the state of Rajasthan using multi-temporal remote sensing data. *International Archives of the Photogrammetry, Remote Sensing & Spatial Information Sciences*.

Sakai, T., Hatta, S., Okumura, M., Hiyama, T., Yamaguchi, Y. and Inoue, G., 2015. Use of Landsat TM/ETM+ to monitor the spatial and temporal extent of spring breakup floods in the

Lena River, Siberia, *International Journal of Remote Sensing*, 36, pp.719-733. doi: 10.1080/01431161.2014.995271.

Sciarone, M., 1998. South African chrome ore for the production of charge chrome. *Geology*, *2*(10), p.1.

Sibanda, M., Mutanga, O., Rouget, M. and Kumar, L., 2017. Estimating biomass of native grass grown under complex management treatments using worldview-3 spectral derivatives. *Remote Sensing*, *9*(1), p.55.

Sohl, T. L. Sleeter, B. M., Zhu, Z., Sayler, K. L., Bennett, K. L., Bouchard, M., Hawbaker, T., Wein, A., Liu, S., Kanengieter, R. and Acevedo, W., (2010). A land-use and land-cover modelling strategy to support a national assessment of carbon stocks and fluxes. *Applied Geography*, 34, pp111-124.

Sorensen, P., 2011. Mining in South Africa: a mature industry?. *International Journal of Environmental Studies*, *68*(5), pp.625-649.

Sothe, C., Almeida, C.M.D., Liesenberg, V. and Schimalski, M.B., 2017. Evaluating Sentinel-2 and Landsat-8 data to map sucessional forest stages in a subtropical forest in Southern Brazil. *Remote Sensing*, *9*(8), p.838.

Suhari, S. and Siebenhüner, M., 1993. Environmental geology for land use and regional planning in the Bandung Basin, West Java, Indonesia. *Journal of Southeast Asian Earth Sciences*, *8*(1), pp.557-566.

Sharaky, A.M., 2014. Mineral resources and exploration in Africa. Department of Natural Resources, Institute of African Research and Studies, Cairo University, Egypt.

Szuster, B.W., Chen, Q. and Borger, M., 2011. A comparison of classification techniques to support land cover and land use analysis in tropical coastal zones. *Applied Geography*, *31*(2), pp.525-532.

Taati, A., Sarmadian, F., Mousavi, A., Pour, C.T.H. and Shahir, A.H.E., 2015. Land use classification using support vector machine and maximum likelihood algorithms by Landsat 5 TM images. *Walailak Journal of Science and Technology (WJST)*, *12*(8), pp.681-687.

Tanser, F.C. and Palmer, A.R., 1999. The application of a remotely-sensed diversity index to monitor degradation patterns in a semi-arid, heterogeneous, South African landscape. *Journal of Arid Environments*, *43*(4), pp.477-484.

Taubenböck, H. and Esch, T., 2011. Remote sensing- An effective data source for urban monitoring. Available online: http://earthzine. org/2011/07/20/remote-sensing-an-effective-data-source-for-urban-monitoring/ [Accessed 10 June 2019].

Thanh Noi, P. and Kappas, M., 2018. Comparison of random forest, k-nearest neighbor, and support vector machine classifiers for land cover classification using Sentinel-2 imagery. *Sensors*, 18(1), p.18.

Thompson, M., 1996. A standard land-cover classification scheme for remote-sensing applications in South Africa. South African Journal of Science, 92(1), pp.34-42.

Tom-Dery, D., Dagben, Z.J. and Cobbina, S.J., 2012. Effect of illegal small-scale mining operations on vegetation cover of arid northern Ghana. *Research Journal of Environmental and Earth Sciences*, *4*(6), pp.674-679.

Tomlinson, C.J., Chapman, L., Thornes, J.E. and Baker, C., 2011. Remote sensing land surface temperature for meteorology and climatology: A review. *Meteorological Applications*, *18*(3), pp.296-306.

Turyahikayo, A., 2015. Assessing land use induced disturbance to vegetation cover in the upper Molopo catchment, South Africa, using Landsat images. In *2015 IEEE International Geoscience and Remote Sensing Symposium (IGARSS)* (pp. 3033-3036). IEEE.

United States Geological Survey (USGS). 2019. USGS high resolution spectral library. [Online]: Available at: https://www.usgs.gov/energy-and-minerals/mineral-resources-program/science/usgs-high-resolution-spectral-library?qt-science_center_objects=0#qt-science_center_objects. [Accessed 25 April 2019].

Verburg, P.H., Van De Steeg, J., Veldkamp, A. and Willemen, L., 2009. From land cover change to land function dynamics: a major challenge to improve land characterization. *Journal of Environmental Management*, *90*(3), pp.1327-1335.

Waylen, P., Southworth, J., Gibbes, C. and Tsai, H., 2014. Time series analysis of land cover change: Developing statistical tools to determine significance of land cover changes in persistence analyses. *Remote Sensing*, *6*(5), pp.4473-4497.

Wessels, K.J., Prince, S.D., Frost, P.E. and Van Zyl, D., 2004. Assessing the effects of human-induced land degradation in the former homelands of northern South Africa with a 1 km AVHRR NDVI time-series. *Remote Sensing of Environment*, *91*(1), pp.47-67.

Wolter, K., 2007. *Introduction to variance estimation*. Springer Science & Business Media.

World Bank, 1994. Making development sustainable: The World Bank Group and the Environment: Fiscal... Washington, DC: World Bank.

Xiuwan, C., 2002. Using remote sensing and GIS to analyse land cover change and its impacts on regional sustainable development. *International Journal of Remote Sensing*, *23*(1), pp.107-124.

Zhu, Y., Chen, S., Wang, Y. and Zhu, Z., 2008. Multi-date satellite images for reducing classification confusion between deciduous forest and evergreen forest. In *2008 International Conference on Computer Science and Software Engineering* (Vol. 6, pp. 85-88). IEEE.